Ann. Phys. (Leipzig) **11** (2002) 8, 573 – 629

Spatial optical (2+1)-dimensional scalar- and vector-solitons in saturable nonlinear media

Carsten Weilnau[1,*], **Marcus Ahles**[2], **Jürgen Petter**[2], **Denis Träger**[1], **Jochen Schröder**[1], **and Cornelia Denz**[1]

[1] Institute of Applied Physics, Westfälische Wilhelms-Universität Münster, Corrensstr. 2/4, 48149 Münster, Germany
[2] Institute of Applied Physics, Technische Universität Darmstadt, Hochschulstr. 6, 64289 Darmstadt, Germany

Received 31 July 2002, accepted 14 August 2002 by U. Eckern

Abstract. (2+1)-dimensional optical spatial solitons have become a major field of research in nonlinear physics throughout the last decade due to their potential in adaptive optical communication technologies. With the help of photorefractive crystals that supply the required type of nonlinearity for soliton generation, we are able to demonstrate experimentally the formation, the dynamic properties, and especially the interaction of solitary waves, which were so far only known from general soliton theory. Among the complex interaction scenarios of scalar solitons, we reveal a distinct behavior denoted as anomalous interaction, which is unique in soliton-supporting systems. Further on, we realize highly parallel, light-induced waveguide configurations based on photorefractive screening solitons that give rise to technical applications towards waveguide couplers and dividers as well as all-optical information processing devices where light is controlled by light itself. Finally, we demonstrate the generation, stability and propagation dynamics of multi-component or vector solitons, multipole transverse optical structures bearing a complex geometry. In analogy to the particle-light dualism of scalar solitons, various types of vector solitons can – in a broader sense – be interpreted as molecules of light.

Keywords: spatial solitons, photorefractive optics
PACS: 42.65.Tg, 05.45.Yv, 42.65.Hw

Contents

* Corresponding author: weilnau@uni-muenster.de

1 Introduction

From our everydays experience, we expect intuitively a wave to spread and broaden as it propagates, like ripples on a lake. In nonlinear physics however, waves can be generated that do not spread or disperse but retain their size and shape indefinitely. They are dynamically and structurally stable objects – so-called *solitons*. The formation and stability of solitons stems from the delicate balance of dispersion and nonlinearity. Dispersion or diffraction drives a wave to spread which can be totally compensated by a nonlinear phenomenon. If the balance between these two competing effects is lost, the generated soliton becomes unstable and, eventually, ceases to exist. In this respect, solitons are completely different from ordinary "linear waves". Solitons can be regarded as a quantity of energy that is permanently confined to a definite region of space or time. It can be set in motion, but does not dissipate by spreading out. In general, when two such waves collide, each comes away from the encounter with its identity being intact. A behavior of this kind is extraordinary, even strange in the frame of

wave physics, but it is familiar in another context. Given a description of an object with these properties, we would call it a particle.

The term soliton was introduced in the 1960's, but the scientific research of solitons had already started in the 19th century when John Scott-Russell observed a large solitary water wave in a canal near Edinburgh. Nowadays, many model equations of nonlinear phenomena are known to possess soliton solutions that have been identified in a large variety of wave and particle systems in nature. Among them are fluids, plasmas, condensed matter waves, particle waves, and even waves in astrophysics. In optics, solitons manifest themselves in two different classes – temporal and spatial solitons. The nonlinearity compensates either for the dispersion-induced spreading of a short light pulse or the spatial divergence of a light beam due to diffraction. The latter scenario is denoted as a spatial soliton which is the main subject of our investigations.

Spatial optical solitons play an outstanding role in nonlinear optics because of their potential of application in optical information processing. In linear optics, the only method to eliminate spatial spreading is to use waveguiding. In a waveguide, the propagation behavior of the beam in a high index medium is modified by the total internal reflection from boundaries with media of lower refractive index. Under conditions of constructive interference between the reflections, the beam becomes trapped between these boundaries and forms a *guided mode*. In nonlinear optics, the effect of light-induced lensing or self-focusing can produce an effective graded index waveguide in which a beam can propagate in a similar non-diffracting way. Intuitively, this can occur when the optical beam modifies the refractive index in such a way that it generates an effective positive lens. As a result, the beam becomes *self-trapped* and its divergence is eliminated altogether, keeping the beam at a very narrow diameter which can be as small as several vacuum wavelengths. Therefore, especially nonlinear optical effects are capable to create waveguiding channels by solitary waves that make spatial optical solitons attractive candidates for novel, adaptive concepts of waveguiding in telecommunication and information processing applications. Nonlinear optics allow the unique possibility to combine the basic features of nonlinear effects with definite applications in information technology.

Among various nonlinear optical systems that are suited for investigations of spatial solitons, the photorefractive medium bears some special features – it has a saturable, but also non-instantaneous, nonlocal and anisotropic nonlinearity. Due to these special features, the investigation of photorefractive spatial solitons allows to prove experimentally many aspects of general soliton theory.

Therefore, the present paper will concentrate on this distinct type of solitary structures, investigating their experimental realization, their stability, their features of interaction as well as their potential for applications in adaptive waveguiding. For this purpose, the paper is structured in the following way: in the introductory Chapter 2, we review the special features of spatial optical solitons, including questions of stability and analytical description. The third chapter is dedicated to the photorefractive nonlinearity and the experimental realization of spatial solitons in two transverse dimensions. The photorefractive effect allows for the first time the experimental investigation of interactions and collisions that have been predicted in soliton- and self-focusing theory several years ago. In Chapter 4 we demonstrate these basic effects in our experimental system. Further on we will show, that the nonlocal and anisotropic feature of the photorefractive nonlinearity supports new, anomalous interaction scenarios for incoherently interacting solitons. In the fifth chapter we will apply these results to realize nonlinear reconfigurable waveguides that allow to process parallel arrays of solitons,

and demonstrate how interaction scenarios can be exploited to realize waveguide couplers and dividers. Therefore, spatial optical solitons represent unique structures that allow to implement novel concepts of how light can be guided and steered by light itself. Finally, we want to extend our investigations to more complex soliton structures that lead to multi-component or vector solitons that are described in Chapter 6. In this way light beams of an elaborate geometry that do not form a solitary structure in nonlinear media by themselves can be stabilized to form a stable non-diffracting object. These complex light structures can be realized in photorefractive media due to the non-instantaneous nature of the effect. We will show that universal features of stability of multipole structures and the decay of structures with phase singularities can experimentally be demonstrated with a photorefractive system.

2 Self-focusing in nonlinear media

A first theoretical investigation of nonlinear optical phenomena in connection with self-trapping of an optical beam was already performed in 1962 by Askaryan [1]. Only two years later, following the first experimental observations by Hercher [2], Chiao [3] could show theoretically that the governing equation of self-focusing is nothing but the nonlinear wave propagation equation with a cubic potential, and that an optical beam can indeed self-trap in such a one-dimensional nonlinear Kerr-medium. He considered a so-called (1+1)-D geometry which indicates that the wave diffracts in one of the two transverse dimensions (x) perpendicular to its propagation direction (z), whereas (2+1)-D denotes the diffraction in both transverse directions (x, y). The index of refraction n of such a medium can be expressed in form of the optical field strength E as

$$n = n_0 + \Delta n(|E|^2) = n_0 + n_2 E^2, \tag{1}$$

where n_0 is the undisturbed linear refractive index, and n_2 is the quadratic term of the nonlinear index variation Δn.

For the case of such a nonlinearity – which is denoted as a Kerr-nonlinearity – exact (1+1)-dimensional self-trapped or solitary waves were consequently found by Zakharov and Shabat [4]. These soliton solutions are more precisely representatives of the class of *bright solitons*, although several other types of solitons as dark solitons – solitary propagation of a dark notch within a spreading light beam – or grey solitons – solitary propagation of a lower light intensity in a higher intensity surrounding – may appear. Details about these other types can e.g. be found in [5].

2.1 The nonlinear Schrödinger equation

In general, the properties of spatial optical solitons with one transverse dimension can be described by the nonlinear wave equation for the beam propagation in a nonlinear medium and the appropriate material equations. The electric field of the optical beam

$$E = \frac{1}{2} A(x, z) \exp(kz - \omega t) + c.c. \tag{2}$$

obeys the wave equation, where $k = \omega n/c$ is the wave number, ω is the frequency of the optical beam and $A(x, z)$ represents the complex slowly varying amplitude of the electric fields, which

is governed by the standard equation

$$i\frac{\partial A}{\partial z} + \frac{1}{2k}\frac{\partial A^2}{\partial x^2} + \frac{kn_2|A|^2}{n_0} \cdot A = 0. \tag{3}$$

Due to its similarity to the well-known Schrödinger equation Eq. (3) is commonly denoted as *nonlinear Schrödinger equation*, where the nonlinear term expresses a trapping potential. Mathematically, the corresponding most simple solitary solution of Eq. (3) is a localized wave packet of the form

$$A(x, z) = \mathrm{sech}(x)\exp(iz/2). \tag{4}$$

This soliton solution $A(x, z)$ can be expanded by introducing the simple transformation $A'(x, z|q) = qA(qx, q^2z)$ with an arbitrary real constant q that leads to a one-parameter space of solutions. Further transformations such as the *Galilean transformation* [6] even lead to a two-parameter family of soliton solutions. The general procedure to solve Eq. (3) is based on the *inverse scattering technique* [4], which can be interpreted as a generalization of the Fourier transform.

The stability properties of a soliton are of immense importance for their physical feasibility. One can prove this property easily by using a stability criterion for soliton solutions of the general nonlinear Schrödinger equation (Eq. (3)). It has been first derived by Kolokov et al. [7–9] (or, for a general review [10]). The validity of this so-called *Vakhitov-Kolokov criterion* is based on the specific properties of the eigenvalue problem that appears after linearizing the nonlinear Schrödinger equation near the solitary solution. If it is fulfilled in the whole parameter space, the soliton solution is stable against small fluctuations.

A linear stability analysis typically does not allow to predict the subsequent evolution of unstable solitons. Therefore, the aspect of stability or instability can be investigated with more complex dynamic studies of the nonlinear wave equation, giving qualitative results about the possible deviation of the initial beam shape from the soliton solution. Recently, the so-called nonlinear theory of soliton instabilities has been suggested in order to give quantitative results about the evolution of unstable solitons [11–13]. This theory is based on the multi-scale asymptotic technique and it allows to describe the soliton evolution near the stability threshold, i.e. the marginal stability curve. According to this approach, unstable bright solitons display three general scenarios of their evolution: they diffract, collapse or switch to a stable state with long-lived oscillations of their amplitude. These *oscillating solitons* are possible due to the existence of soliton internal modes, one of the major properties that separates integrable and non-integrable models.

The nonlinear Schrödinger equation (Eq. (3)) is integrable owing to the fact that it has an infinite number of conserved quantities. Especially, due to this property, the striking feature of its soliton solutions manifests in their interaction behavior. Solitons of the nonlinear Schrödinger equation not only conserve energy and velocity upon collision, but also maintain their transverse shape and their identity. Hence the number of solitons is conserved, and all interaction scenarios display a fully elastic behavior.

2.2 Extensions to non-Kerr media

The idealized situation of a Kerr-like nonlinear medium does not include a wealth of phenomena that appear during self-trapping of optical beams in real nonlinear optical media, due to

two main factors: higher-order nonlinearities and higher degrees of freedom of the nonlinear medium. In many cases, higher intensities give rise to a field-induced change in the refractive index that is influenced by higher-order nonlinearities. Often, the nonlinearity is of a cubic-quintic type as i.e. $\Delta n(|A|^2) = n_2|A|^2 + n_4|A|^4$, which results not only in self-trapping but gives rise to resonant four-wave mixing effects between the fundamental and a secondary field. As long as the higher-order nonlinearity is stronger than the cubic one, i.e. a power-law focusing, the nonlinear Schrödinger equation has localized solutions which blow-up, so that a singularity appears at finite z and the so-called catastrophic self-focusing or self-focusing collapse takes place.

Another source of phenomena beyond Kerr-like solitons is due to the surroundings of the beam that may include more dimensions of freedom than the soliton itself needs for stable propagation, giving rise to a broader class of perturbations and therefore instabilities of the solitary wave solution. They are the reasons why in (2+1) dimensions, Kerr-nonlinearities do not support the formation of a stable solitary wave. For two transverse dimensions in bulk media the cubic nonlinear Schrödinger equation predicts a catastrophic unlimited self-focusing, which leads to a random filamentation of an optical beam with an initial power larger than the critical power of self-focusing [14]. In the following, we will discuss especially this aspect and the changes it introduces to the possibility of spatial soliton formation compared to the case of the Kerr-nonlinearity soliton.

2.3 Solitons in two-dimensional saturable systems

A key to the problem of self-focusing collapse and formation of filamentation is the change in the nonlinearity. By introducing an upper limit for a Kerr-like nonlinearity stable self-focusing in both transverse dimensions can be achieved [15]. Therefore, a saturable nonlinear behavior is a prerequisite for solitary beam formation in bulk media. In order to take into account this saturation behavior, the beam propagation by Eq. (3) can be described by the modified nonlinearity

$$\Delta n = -\Delta n_{\max} \frac{1}{1 + |A|^2/I_{\mathrm{sat}}}. \tag{5}$$

Here, $\Delta n_{\max}$ denotes the maximum refractive index change. When the field intensity given by $|A|^2$ is much smaller than the saturation intensity I_{sat} the system operates in a Kerr-regime and $\Delta n \propto |A|^2$. In the other limit, for $|A|^2 \gg I_{\mathrm{sat}}$ the refractive index change decreases and thereby prevents the catastrophic collapse of the light beam. Because of this Kerr-like but saturable characteristics of the nonlinearity, a stable self-focusing of a light beam in both transverse dimensions can be realized.

Such a model can be used for the description of an off-resonant interaction of the optical beam with an atomic system (e.g. semiconductor-doped glasses with highly nonlinear optical properties) as well as for self-trapping due to saturation of the ac Stark shift of two-photon states. Moreover, we will show in chapter 3.1 that the formation of all photorefractive solitons can in principle be described with such a model.

The modification of the nonlinearity from Kerr- to a saturable Kerr-like nonlinearity brings along some dramatic consequences for the solitary solutions of the system. The equation is no longer integrable, so that in general analytical soliton solutions to Eq. 3 do not exist any more. In contrast to the one-dimensional integrable system that has an infinite number of

conserved quantities, the saturable system has only a limited number of conserved quantities. Among those are the three lowest order conserved quantities energy Q, momentum M, and the Hamiltonian H [6]. Even though a system is not necessarily integrable it can still be classified as Hamiltonian [6] as long as stationary solitary solutions can be found and shown to be stable by a linear stability analysis.

Probably the most striking feature of solitons in nonlinear saturable system shows up in their interaction behavior. Whereas soliton solutions of the (1+1)-dimensional Kerr system are characterized by elastic collisions, energy- and particle conservation, solutions of saturable systems display in general non-conservative properties, such as radiation dissipation, shape transformation and even merging- and fission-processes upon collisions. Additionally, a whole variety of soliton-like solutions exists that might be stable or unstable depending on their specific parameters [16]. Although these distinct properties are in contradiction with a particle-like behavior, the label ' soliton ' is commonly used to describe various kinds of self-trapped beams and pulses in models which are in fact non-integrable. The reader should keep this in mind when we refer to solitons in two-dimensional transverse systems throughout the following text. These are only solitary waves, but not soliton solution, according to the strict mathematical definition.

2.3.1 Theory of (2+1)-D solitons in saturable media

Stable self-focusing of a light beam in two transverse dimensions has been realized in a variety of physical systems that supply a saturable nonlinear refractive index change. The first experiment dates back to 1974 where Bjorkholm and Ashkin [17] succeeded in self-trapping a circular cw-laser beam in atomic sodium vapor. In the early nineties the existence of solitons in photorefractive crystals has been predicted [18] and subsequently verified in an experiment [19]. Nowadays, photorefractive crystals have become the material of choice to investigate the generation, stability, interaction, and dynamical processes of spatial solitons [5, 20]. This specific system is the main subject of our investigation and it will intensively be described in Section 3.1. For a recent review on spatial solitons in general, we refer to [21, 22].

Here, we focus on the universal theory of solitary beam formation in a bulk saturable nonlinear medium and describe its basic characteristics. Starting from the standard paraxial approximation of the wave equation in a nonlinear material [23]

$$i\frac{\partial A}{\partial z} + \frac{1}{2k}\nabla_\perp^2 A + \frac{k\Delta n(I)}{n_0}A = 0, \tag{6}$$

where $\nabla_\perp^2$ represents the transverse Laplacian ($\partial^2/\partial x^2 + \partial^2/\partial y^2$), and z is the direction of propagation, respectively. A general wave equation can be derived for propagation in a saturable nonlinear medium by inserting Eq. (5) into Eq. (6). When scaling the spatial coordinates to $\xi = \frac{z}{kx_0^2}$, $x' = x/x_0, y' = y/x_0$, and the amplitude to $\tilde{A} = A/\sqrt{I_{\rm sat}}$, we obtain a normalized propagation equation for a saturable isotropic nonlinear medium:

$$i\frac{\partial \tilde{A}}{\partial \xi} + \frac{1}{2}\nabla_{\perp'}^2 \tilde{A} - \gamma\frac{\tilde{A}}{1+|\tilde{A}|^2} = 0, \tag{7}$$

where we define a coupling parameter γ that depends on the specific physical system and describes the impact and the specific material constants of the nonlinear medium. When x_0 is chosen to be the initial width of the incident light beam, kx_0^2 equals the diffraction length

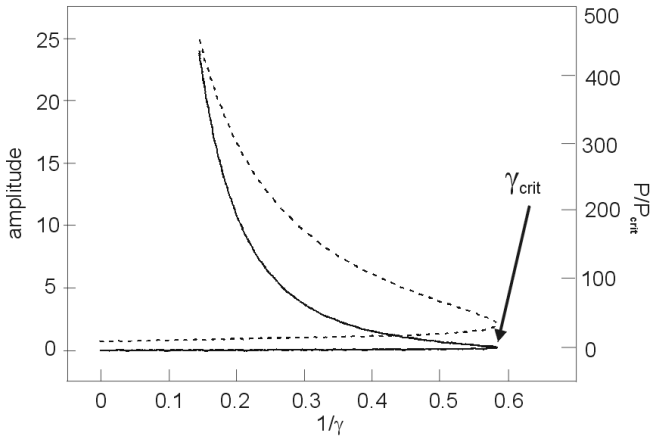

Fig. 1 Numerically calculated (2+1)-D soliton solutions for a saturable nonlinear medium. Dependence of the soliton amplitude (dashed curve) and normalized soliton power (solid curve) on the coupling parameter γ (after Gatz and Herrmann [24])

L_d of an appropriate Gaussian beam. Therefore, in simulations the propagation distance ξ is commonly expressed in terms of the diffraction length which always gives an indication how strong the beam would have spread if it was propagating in a linear medium.

The solution of the wave equation (Eq. (7)) can no longer be found analytically, which is the major difference to the nonlinear Schrödinger equation (Eq. (3)). With the boundary condition of $I(x, y) \to 0$ for $x, y \to \pm\infty$ and the radially symmetric ansatz

$$A(\xi, r) = \rho(r) \cdot \exp(i\varphi\xi), \tag{8}$$

Gatz and Hermann [24] solved the resulting propagation equation numerically with an iterative procedure. Thereby they were able to derive a whole family of soliton solutions. In these solutions, the amplitude ρ is independent of the propagation coordinate ξ, which implies that it does not vary as the beam propagates in the ξ direction, whereas $\exp(i\varphi\xi)$ represents a uniform phase factor that varies only with ξ but is independent of the radial coordinate $r = \sqrt{x'^2 + y'^2}$. Solitary solutions exist for any $\gamma > \gamma_{\mathrm{crit}} = 1.69$, which is illustrated by the arrow in Fig. 1.

The most striking phenomenon is that the soliton amplitude becomes a two-valued function of the parameter γ depending on the soliton width. From the two-valued curve that is shown in Fig. 1 it is evident that for an arbitrary $\gamma > \gamma_{\mathrm{crit}}$ there exist two soliton solutions with different amplitude and power for the same γ. Such a property is similar to that in optical bistable systems: there exist two possible (output) soliton states for the same value of an input parameter. Therefore, we denote the soliton solution of Eq. (7) as bistable solitons. In the specific physical system of [24] the initial beam width x_0 is proportional to γ and therefore a minimum beam width exists for the soliton to be stabilized. This remarkable fact does not exist for non-saturable Kerr nonlinearities.

2.3.2 Stability of two-dimensional soliton solutions

The numerically calculated transversal shape $\rho(r)$ of the derived solutions is almost Gaussian, the deviations are within a range which is smaller than 5%. Starting from a Gaussian intensity distribution, a dynamical analysis by applying the *beam propagation method* [25] reveals, on the one hand, that a Gaussian beam with the appropriate choice of parameters does indeed self-trap. On the other hand, the formation of a solitary solution is always accompanied by oscillations of the beam's amplitude and width as it propagates in the positive ξ direction.

This oscillatory behavior represents a constant reshaping process and stems from the slight deviations from the numerically derived soliton solution. It depends strongly on the coupling parameter γ as well as on the initial beam power. For $\gamma \leq 2$ the on-axis intensity deviations do not exceed 10% from the soliton peak intensity. For larger coupling parameters $\gamma \geq 2$, the deviations become more dramatic and may even prevent a reshaping into a solitary solution, the beam becomes subject to diffraction.

In contrast to solitons in (1+1)-D Kerr-systems this effect is not of transient nature. In a Kerr-medium, beams with a transverse Gaussian profile converge into a stable soliton solution after a certain propagation distance even if their initial parameters deviate up to 50% from those of the soliton solution. In saturable (2+1)-D systems such a convergence from a Gaussian beam into a soliton solution does in fact not exist. When the beam intensity and the coupling parameter are within a certain range, self-focused light structures evolve from incident Gaussian beams, but during propagation the beam undergoes a permanent reshaping process and shows non-vanishing oscillations around the stable soliton solution [24].

2.3.3 General interaction features of (2+1)-D solitons

The most remarkable feature of solitons in saturable systems is manifest in their interaction behavior. In general, the beams do not remain unaffected when they pass through each other and the number of solitary beams is not necessarily conserved. These effects mainly depend on the collision angle and the relative phase of the colliding beams. To classify this feature, a critical colliding angle θ_{cr} can be defined which is in analogy to the critical angle of total internal reflection of a linear waveguide [26]. When two beams with a phase difference of $\varphi = 0$ collide at a shallow angle $\theta < \theta_{cr}$, they can fuse into a single beam that in turn may display strong oscillations, depending on the initial conditions. By changing the relative phase to an intermediate value between 0 and π, a deflection of both beams can take place and with increasing propagation their amplitudes may change periodically. When the beams are finally out of phase by π, they repel each other and their transverse profile remains unaffected by the collision process.

The situation changes dramatically when the collision angle θ exceeds the critical angle θ_{cr}. Now, the solitons intersect and display an inelastic collision process which again induces strong oscillations along the propagation direction. Depending on the relative phase, energy will be transferred between the two components that leads to an asymmetric intensity distribution [24]. Eventually one beam merges completely into the other one. An intriguing effect takes place in the highly saturated regime when the intersection angle is $\theta \approx \theta_{cr}$. In this specific case an additional solitary beam can be created due to the collision process [26] and three beams may emerge from the collision center.

All interaction processes in bulk saturable media imply a certain dissipation of energy in form of radiation. The energy within the solitary solutions is not conserved anymore, and collisions are inelastic in contrast to Kerr-systems. The deviation from the initial soliton profile due to radiation losses finally leads to the oscillating behavior described above. All three interaction processes are universal for all saturable nonlinear systems [27–32], and most of their features will be described more precisely by means of the photorefractive system in Section 4.

2.4 Vector solitons

Using the linear optical model of waveguiding to describe spatial soliton formation in two dimensions, a two step process can be identified. First, a light beam which is incident on a self-focusing saturable nonlinear medium induces a focusing refractive index structure. In a second step, once the waveguide has been formed, it supports the non-diffracting propagation of its eigenmodes. When the incident light beam coincides with the eigenmode of its induced waveguide, the beam itself will be trapped and propagate with an invariant transverse profile. This principle of self-consistency has been developed by Snyder et al. [33,34] and gives a very intuitive insight into the soliton formation process.

So far we only described a single optical beam that induces a waveguide structure in which it propagates as a fundamental mode. This is commonly denoted as a *scalar soliton*. In contrast, if the refractive index waveguide is induced by several simultaneously propagating optical beams and therefore represents a multi-mode waveguide structure, in which all invoking beams can propagate as eigenmodes, the joint light structure is denoted as a *vector* or *multi-component* soliton. This type of solitons has been suggested by Manakov [35] in the case of a one-dimensional Kerr-system and has been realized experimentally in a semiconductor material [36]. We investigate these structures in chapter 6 in their extension to two transverse dimensions and show how these structures can be realized and stabilized.

The most important prerequisite for the generation of this new and fascinating type of optical solitary waves is the absence of any interference between the several optical beams. Moreover, self- and cross-phase modulation terms have to be equal for all contributing components. Thus, the refractive index change which is induced by a distinct beam affects every propagating light component in exactly the same way. The coupling between single solitary beams is only due to the nonlinear response of the medium to the beams' optical intensity distribution.

In general, there exist three ways to achieve these requirements. The original suggestion of Manakov is based on two beams with orthogonal states of polarization. A second approach can be realized by applying two beams of different wavelength as for the case of all quadratic solitons [37]. Finally, using mutually incoherent beams is a very convenient way to realize multi-component solitary waves especially in photorefractive systems, as will be shown in chapter 6. Vector- or multi-component solitons inhibit an enormous potential towards future applications since the single contributing light components can display different geometries that give rise to rather complex scenarios. Moreover, higher-order multicomponent solitons are utilized to describe spatially incoherent beams, therefore opening an insight into the question whether an incoherent, white-light soliton can be formed and stabilized.

We will show in the next chapter that certain relations that have been described in this chapter also exist for the most interesting and realistic experimental example of (2+1)-D spatial soliton – the generation of photorefractive spatial screening solitons.

3 Solitons in photorefractive crystals

The most promising new type of spatial solitary waves are spatial solitons realized by the photorefractive nonlinearity in an electro-optic crystal. The first type of such a photorefractive soliton that has been studied stems from the nonlocal nature of the photorefractive effect and is transient by nature [19]. It is named *quasi-steady-state soliton*. A second type of photorefractive soliton, denoted as a *screening soliton*, appears in the steady-state and is associated with

an intensity-dependent screening of an external electric field [38–40]. Finally, in photovoltaic materials, a third type of spatial soliton can be generated without the need of an external biasing field [41, 42].

The most attractive property of these spatial solitons in photorefractive materials is the very low laser power in the range of a few microwatts that is necessary for their generation. This shifts the investigations of spatial solitons to a power region that is accessible with conventional cw-laser sources, and allows for the first time to think about realistic applications for waveguiding and switching due to the ease of availability, compactness and relatively low costs of the experimental devices. Therefore, there has been an exploding interest in this new type of spatial solitons within the last decade.

In a photorefractive medium with an external bias electric field oriented along one of the transverse axes, an optical beam propagating along the z-axis changes the refractive index due to the generation of free charge carriers and the subsequent creation of a space charge field by the light-matter interaction inside the material. Because the optically induced space charge field screens the externally applied electric field, the effective refractive index in a photorefractive crystal becomes a nonlinear function of the light intensity I, of the type that is analogous to a saturable nonlinearity. Consequently, photorefractive screening solitons are the most attractive candidates to prove numerous conclusions drawn from theoretical investigations in an experiment. In that way, they represent the driving motor of recent theoretical attempts to describe (2+1)-D spatial soliton formation in saturable media. In order to understand the behavior of this attractive and new kind of spatial solitons, and to exploit them for investigations of the basic nature of (2+1)-D spatial solitons, we first focus in Section 3.1 on the photorefractive nonlinearity in detail before we describe the experimental implementations in Section 3.4.2.

3.1 General features of the photorefractive nonlinearity

The photorefractive effect has been discovered in $LiNbO_3$ crystals and was first denoted as an *optical damage* [43], since the wavefront of a coherent light beam propagating in the crystal became strongly affected. Since then, the effect has been observed in many different crystals such as: $BaTiO_3$, SBN, $KNbO_3$, KTN, BSO, GaAs, and InP. These typically non-centrosymmetric materials exhibit a $\chi^{(2)}$-nonlinear response and their light-induced refractive index change can grow up to the order of magnitude of $\Delta n \approx 10^{-5}$. The generic physical process can be explained by a two-step mechanism. First, the crystals are photoconductive, which means that free charge carriers can be generated due to light illumination. The electrons or holes become mobile in the crystal's conduction band and may migrate to non-illuminated regions where they recombine with impurities. In this way an electrostatic field $E_{\rm sc}$ builds up and due to the linear electrooptic effect, which is also denoted as Pockels effect, the material's refractive index will be modulated according to:

$$\Delta n = -\frac{1}{2} n_o^3 r_{\rm eff} E_{\rm sc}, \tag{9}$$

where $r_{\rm eff}$ represents an effective electro-optic coefficient, which depends on the specific light polarization and the crystal's lattice geometry. The photoconductive properties can be designed by inducing a distinct type of impurity atoms that act as charge donors or acceptors, respectively.

When the crystal is subject to a local light illumination, electrons (which are considered here as the relevant charge carriers) can be excited from donor atoms into the crystal's conduction

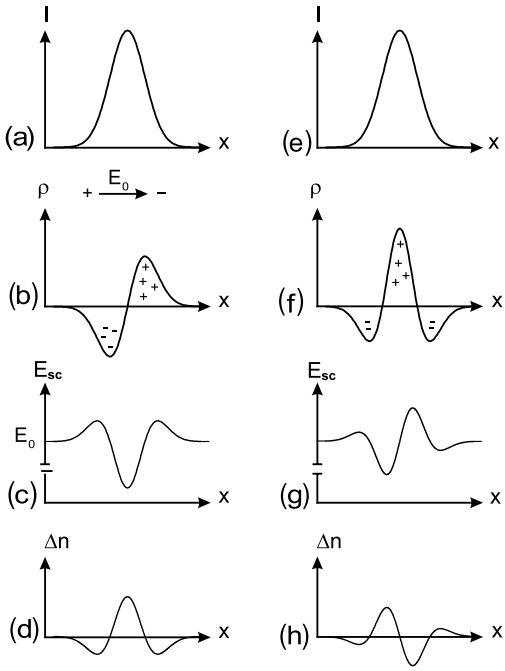

Fig. 2 Sketch of drift and diffusion-dominated charge carrier transport process and its impact on the induced refractive index modulation. Light intensity pattern (a,e), charge density (b,f), space-charge field (c,g), and refractive index modulation (d,h) for a drift or a diffusion process in the left and right column, respectively

band in case the photon energy is large enough. The resulting ionized donors serve as trap centers that may recapture the free electrons. The excited free electrons in turn become mobile and might either be captured by the ionized donors or they move towards non-illuminated regions where they can be trapped by acceptor atoms.

This redistribution of electrons is due to two different charge carrier transport processes, namely drift in an external or photovoltaic electric field and diffusion. It brings along the built up of a static space charge field E_{sc} which in turn is responsible for the desired refractive index modulation. Although the typical time constants of electron excitation and recombination as well as their migration in the conduction band are on a short time scale, the duration of the built up process of the space charge field varies from milliseconds up to a few seconds. This relatively long time interval stems from the fact that a relatively large amount of charge carriers has to migrate until a state of equilibrium and hence a relatively strong electric space charge field is created.

To gain insight into the relevant details we qualitatively explain the separate influence of drift and diffusion effects on the generation of the space charge field and hence the refractive index modulation. Fig. 2 demonstrates the impact of a drift-dominated charge carrier transport process on the refractive index modulation in the left column (Fig. 2(a)–(d)) and the effect of a diffusion-dominated process in the right column (Fig. 2(e)–(h)). Starting from a Gaussian intensity distribution in Fig. 2(a), electrons from the central area will be excited into the conduction band. Due to the presence of an external electric field E_0 as depicted in Fig. 2(b), the electrons will drift into a defined direction, and the resulting charge density ρ becomes asymmetric. By integrating $\rho(x)$ one can derive the optically induced space charge field E_{sc} (Fig. 2(c)) which transforms into a symmetric elevated refractive index modulation Δn (Fig. 2(d)) via the Pockels effect given by Eq. (9). In this case the light intensity pattern in

Fig. 2(a) induces a positive refractive index modulation that resembles a focusing structure. When the external electric field in Fig. 2(c) points in the other direction, the opposite effect takes place, and the net refractive index change will be negative leading to a de-focusing refractive index profile that allows for the generation of dark solitons.

In the right column, the impact of diffusion on the induced refractive index change is illustrated. Starting from the same intensity distribution in Fig. 2(e), the electrons diffuse symmetrically to areas of lower light intensity in the vicinity if the optical beam. The resulting space charge field in Fig. 2(f) is asymmetric and the net refractive index change in Fig. 2(h) represents more an asymmetric and deflecting than a symmetric and focusing structure. From this simple illustration it is clear that both effects, diffusion and drift induce different types of refractive index changes, which can never be separated in a real physical system. To obtain a focusing refractive index structure, the charge carrier transport process has to be drift-dominated. Therefore, the crystal has to be biased by a dc-electric field in typical experimental setups for the generation of photorefractive screening solitons. However, the diffusion process is always present, and the net refractive index change consists of contributions from both – the drift and the diffusion effect. This situation is reflected in a self-focusing effect that is accompanied by a lateral shift of the beam while propagating in the nonlinear medium. This effect is commonly denoted as bending [44, 45].

3.2 The band transport model

To describe the charge transport processes quantitatively, we rely on a description based on the band transport model that has been derived by N. Kukhtarev et al. [46] in 1979. Suppose we have a light intensity pattern I incident on a photorefractive crystal. In the steady state the rate of generation of free charge carriers equals the recombination rate:

$$(\beta + sI)(N_D - N_D^+) - \gamma_r n_e N_D^+ = 0, \tag{10}$$

where N_D^+ is the density of ionized donor atoms, N_D is the density of the donor impurities and n_e represents the density of free electrons. The optical and thermal excitation coefficients are represented by s and β, respectively, and the recombination coefficient is given by γ_r. The net charge density ρ is connected to a current density j via the continuity equation

$$\partial\rho/\partial t = -\nabla \mathbf{j} = 0 \tag{11}$$

and equals zero, because the system is in a steady state. Assuming that $\mathbf{j}$ consists only of the two components – drift and diffusion – and neglecting the photovoltaic term, we express the current density as a function of the electron density n_e and the static space charge field E_{sc}

$$\mathbf{j} = e\mu_e n_e \mathbf{E}_{\mathrm{sc}} + \mu_e k_n T \nabla n_e. \tag{12}$$

Here, e and μ_e are the unit charge and electron mobility, k_B is the Boltzman constant, and T describes the absolute temperature. The first term of Eq. (12) represents the drift of electrons due to an electric field and the second term describes the diffusion process. Since Eqs. (10–12) can not be solved analytically, several approximations have to be made in order to derive an expression for the space charge field. Throughout this article we will illustrate numerical results that are based on two different approaches that are denoted as isotropic and anisotropic, respectively.

3.2.1 Isotropic approximation of the space charge field

The isotropic approximation to solve Eqs. (10-12) is described in detail in [39]. It starts with a normalization of the beam intensity I in Eq. (10) relative to the so-called dark intensity $I_d = \beta/s$ which in turn represents the ratio of the thermal- to the photoionization coefficient. In our experiments, the crystal is illuminated with a homogeneous white light source to control its degree of saturation, which represents an artificial tool to tune the dark and thermal conductivity of the material. This affects the generation of free electrons, but can be considered to be equivalent to a thermal excitation.

According to Christodoulides [39], we assume that the optical intensity asymptotically attains a constant value at the crystal border, and can be expressed by $I(x \to \pm\infty, z) = I_\infty$. In these regions of homogeneous intensity we also assume the space charge field to be independent of the transverse coordinates x, y, i.e. $E_{\rm sc}(x \to \pm\infty, z) = E_0$. When the spatial extent of the light wave is much smaller than the width of the crystal L, which is biased by an external voltage V, the space charge field at the crystal border E_0 is approximately V/L. Under strong bias conditions, where $E_0 = V/L$ will reach appreciable values and the drift component of the space charge field will be dominant, so that the diffusion terms can be neglected, Eqs. (10-12) can be processed to derive an expression for the space charge field

$$E_{\rm sc} = E_0 \frac{I_\infty + I_d}{I + I_d}. \tag{13}$$

Note the isotropic character of the derived expression, because $E_{\rm sc}$ is only dependent on the intensity distribution but not on any spatial coordinates. If we now assume that $I_\infty = 0$, which is reasonable for the case of soliton investigations in photorefractive materials, we can directly insert Eq. (13) into Eq. (9). The resulting expression for the refractive index modulation Δn can then finally be inserted into Eq.(6). Successively performing the usual scaling transformation which is described in Section 2.3.1 and defining I_d as saturation intensity $I_{\rm sat}$, we can scale $\tilde{A} = A\sqrt{I_d}$ and end up exactly with the same equation as the general equation of beam propagation in a saturable nonlinear medium given by Eq. (7). Since we now deal with a specific physical system, the coupling parameter γ takes the definite form of

$$\gamma = \frac{1}{2} k_0^2 x_0^2 n_0^4 r_{\rm eff} E_0. \tag{14}$$

Even though we apply an external voltage of $V/L = E_0$ along the horizontal x-axis, the propagation equation remains isotropic and the strength of the nonlinearity which is given by γ depends only on the external electric field E_0. The optically induced space charge field, which is given through Eq. (13) is proportional to the external field but does not depend on any spatial transverse coordinates.

3.2.2 Anisotropic approximation of the space charge field

The second major approach – which is commonly denoted as anisotropic – describes the space charge field of the material in a more complicated way. The model was introduced by Zozulya and Anderson [47] and is based on the simple assumption that the space charge field can be expressed in terms of an electrostatic potential $E_{\rm sc} = -\nabla\phi$. With this relation one can rewrite Eq. (12) as

$$j = -e\mu_e n_e \nabla\phi + \mu_e k_B T \nabla n_e. \tag{15}$$

Assuming a quasi-uniform illumination, indicating that the spatial variation of the light intensity exceeds by far the drift and diffusion length of the electrons in the conduction band, the local charge density equals zero

$$\rho = N_A + n_e + N_D^+ = 0, \tag{16}$$

with N_A being the acceptor density. Assuming further that the density of the free electrons is negligible compared to the acceptor density, $n_e \ll N_A$ and that the rate of generation of free electrons is much smaller than the recombination rate $(\beta + sI) \ll \gamma_r N_a$ one can derive a simple expression for the electron density [23]:

$$n_e = \frac{N_D - N_A}{\gamma_r N_A}(\beta + sI). \tag{17}$$

As in the isotropic approach, it is convenient to normalize the beam intensity I by I_d. From Eq. (17) we express the electron density by

$$\frac{N_D - N_A}{\gamma_r N_A}\beta(1 + I/I_d) = \frac{N_D - N_A}{\gamma_r N_A}\beta(1 + \hat{I}), \tag{18}$$

and neglect the $\hat{}$-sign in the following. Inserting Eq. (18) and Eq. (12) into Eq. (10) yields:

$$\nabla I \nabla\phi + (1 + I)\nabla \cdot (\nabla\phi) - \frac{k_B T}{e}\nabla^2(1 + I) = 0. \tag{19}$$

Since we apply an external electric field along the positive x-direction, it is appropriate to assume that the electrostatic potential consists of a light induced term ϕ_0 and an external bias term $-E_0 x$. Inserting $\phi = \phi_0 - E_0 x$ into Eq. 19 and dividing by $(1+I)$ leads to an expression of the potential equation for the electrostatic field:

$$\nabla^2\phi_0 = -\nabla \ln(1+I)\nabla\phi_0 + E_0\partial/\partial x \ln(1+I) - \frac{k_B T}{e}[\nabla^2 \ln(1+I) + (\nabla \ln(1+I))^2]. \tag{20}$$

With this specific type of nonlinearity the space charge field $E_{\rm sc} = E_0 - \nabla\phi$ can be expressed in terms of the externally applied voltage V with $V/L = E_0$ and by the light induced electrostatic potential ϕ_0 which can be calculated from Eq. (20).

Eq. (20) contains both contributions to the space charge field – drift and diffusion. The first one is represented by the second term of the right side of Eq. (20), whereas diffusion is described by the last term on the right side of Eq. (20).

Inserting the expression for $E_{\rm sc}$ into Eq. (9) and include the resulting refractive index modulation Δn into Eq. (6) yields a propagation equation for an optical beam in a biased photorefractive medium which can be written as

$$i\frac{\partial A}{\partial \xi} + \frac{1}{2}\nabla^2_{\perp'} A - \gamma(1 - \nabla\phi_0/E_0)A = 0. \tag{21}$$

Note that the amplitude is again scaled with the dark intensity as $\tilde{A} = A/\sqrt{I_d}$ and $AA^* = I$. All other parameters and scaling constants are unaltered compared to the isotropic and saturable case expressed by Eqs. (7,14). The potential ϕ_0 can be calculated from Eq. (20) numerically

for a given intensity distribution. It can then be inserted into the nonlinear term of Eq. (21) allowing to find solitary solutions.

The saturable characteristics of the nonlinear term of Eq. (21) is not as obvious as in the isotropic case given by Eq. (7). Its origin lies in the nature of the photorefractive effect which is directly dependent on the generation of free electrons due to the formation of the space charge field and hence the refractive index. Because the number of donor atoms is finite, there always exists an equilibrium between electron generation and recombination. Therefore, the space charge field and consequently the refractive index modulation display an upper threshold. Comparing Eq. (21) with the standard equation of beam propagation in a nonlinear medium (Eq. (6)), it is obvious that the external field decreases the refractive index globally whereas the light induced potential leads to a positive refractive index change. The externally applied field E_0 is screened by the photoinduced charge carriers, which gives rise to screening soliton generation.

The most important aspect of applying the complete photorefractive approach expressed in Eqs. (20, 21) is that the anisotropic nature of the system is seriously affecting the formation of solitary beams. From the simple sketch in Fig. 2 it is obvious that the charge carrier process has to be drift dominated to create a focusing refractive index structure. Applying an external electric field in one transverse direction inherently introduces a symmetry-breaking of the system, thereby destroying the isotropic situation. This aspect is only taken into account by the anisotropic model since Eq. (20) bears a derivative with respect to the transverse coordinate x. The diffusion as the second charge carrier transport process is neglected in the isotropic approach in Section 3.2.1 but represented by the last term ($\propto k_B T/e$) of Eq. (20) in the anisotropic model. Therefore, the anisotropic approach represents the propagation of an optical beam in a photorefractive crystal in a more realistic way than the isotropic model. Nevertheless, the isotropic model is able to demonstrate the most general features of soliton formation and interaction. Since it can be described by just one propagation equation (Eq. (7)), it requires less computational resources than the anisotropic model that consists of an additional equation for the electrostatic potential (Eqs. (20),(21)).

To summarize, the photorefractive nonlinearity exhibits some special features that are well-suited for investigations of spatial solitons. The most important aspects can be summarized as:

- Photorefractive materials exhibit a nonlocal light-matter interaction, leading to a response to the optical beam that is broader than the tails of the beam. This nonlocality leads to different unexpected effects in soliton interactions.

- Photorefractive materials react non-instantaneously on the light radiation, because the formation of a significant refractive index modulation is connected with a high space charge field.

- The propagation of an axially symmetric beam propagating in a photorefractive medium can lead under certain conditions to self-focusing that corresponds to an effective optical lens with astigmatism. This is mainly due to the fact that the external electric field induces an anisotropy in the process. The deviation from the isotropic model therefore becomes different for the two transverse directions, leading to astonishing effects of solitary beam formation.

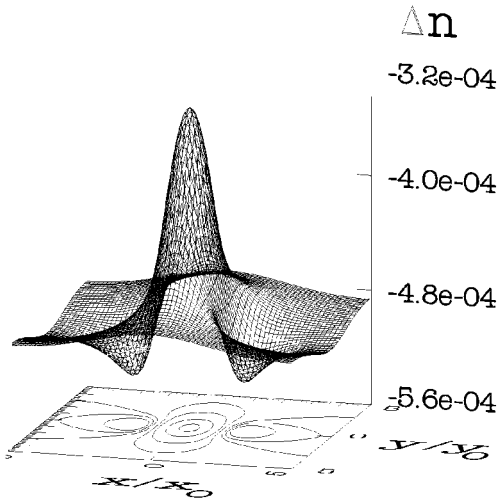

Fig. 3 Three-dimensional plot of the refractive index modulation. The symmetry-breaking impact of the electric field applied along the x-direction is clearly visible, leading to defocusing domains along the x-axis

- The photorefractive nonlinearity exhibits additional effects such as self-bending of solitary beams during propagation due to diffusion effects that interplay with the effects of drift due to the externally applied electric field or a possible polarization coupling process.

3.3 Features of the photorefractive index modulation

Starting from a Gaussian intensity profile one can solve Eq. (20) numerically with the help of a relaxation technique [48]. A three-dimensional plot of the resulting refractive index modulation for $r_{\mathrm{eff}} = 235$ pm/V, $n_0 = 2.3$, $x_0 = y_0 = 15$ µm, $\lambda = 532$ nm and $V = 3$ kV, is depicted in Fig. 3. In this simulation we neglect the diffusion term in Eq.(20) and illustrate only the effect of a drift-dominated charge carrier transport. According to Fig. 3 the anisotropic nature of the refractive index modulation reveals clearly. It is not circular symmetric as its provoking light intensity distribution. Remarkably, along the x-direction, the refractive index has focusing as well as defocusing areas at the margins of the beam. In Fig. 4 we illustrate this peculiar phenomenon more detailed since it represents the key to all subsequent effects of screening soliton generation and interaction in photorefractive crystals.

Let us consider a Gaussian intensity distribution in Fig. 4(a) and its appropriate refractive index modulation in Fig. 4(b) as a 2-dimensional plot. Figs. 4(c) and (d) illustrate the two transverse cross sections of the modulation along the x- and y-direction respectively. Comparing the frames of Fig. 4(a) and (b), the non-local nature of the refractive index modulation becomes obvious. It even changes in non-illuminated regions away from the center of the beam. The cross section along x for $y = 0$ (Fig. 4(c)) shows that the refractive index increases only in the central region of the beam but even decreases at its border. In the horizontal border regions, the material acts in a rather defocusing way, but the cross section along y (perpendicular to the external field) for $x = 0$ (Fig. 4(d)) displays a focusing structure everywhere. Taking also into account the diffusion of charge carriers, the scenario gets even more complicated. A more detailed analysis of the impact of both effects – diffusion and drift – on the refractive index modulation can be found in [47]. Generally speaking, the diffusion process induces an

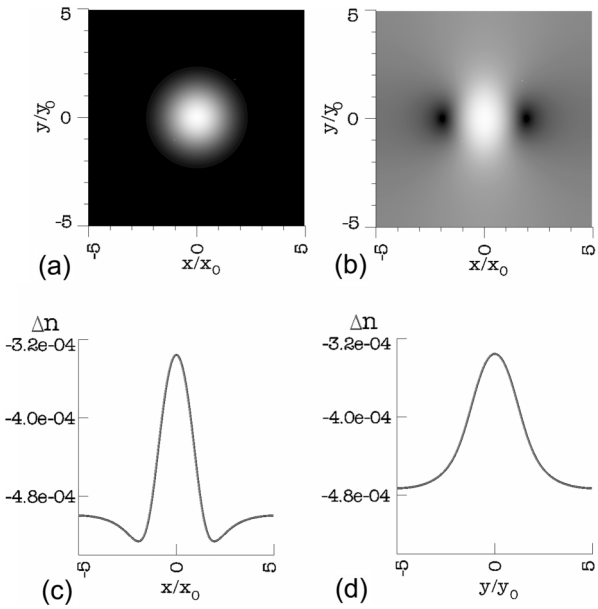

Fig. 4 Two dimensional plots of Gaussian intensity distribution (a) and its appropriate refractive index modulation (b). Plots of the cross sections through the center along x (c) and y (d)

asymmetric deformation of the focusing refractive index profile in a way depicted by Fig. 2(h). Even though this leads to a lateral deflection of the beam it has no impact on the self-focusing property in principle. The non-local, anisotropic and non-instantaneous nature of the optically-induced refractive index modulation gives rise to a variety of distinct properties and effects of photorefractive screening solitons that will be the focus of the next section.

3.4 Screening photorefractive soliton formation

3.4.1 Theory

Exact numerical solutions to Eqs. (20,21) can be found by applying a numerical procedure suggested by Petviashvili [49, 50]. For soliton solutions one can make an ansatz equivalent to the one in Section 2.2 that the amplitude is independent of the propagation coordinate ξ, and that only the phase varies with ξ but is independent of the radial coordinates x and y. The Petviashvili-method does not imply any further approximations, but transforms the equations into a fix point problem that can be solved iteratively. A contour plot of the solution of Eqs. (20),(21) for $E_0 = 2\,\mathrm{kV/cm}$ is depicted in Fig. 5(a). It shows an exact soliton solution, with the special feature that the beam shape is rather elliptical than radially symmetric as one might already expect from the anisotropic refractive index change in Fig. 3. Although the simulation neglects diffusion, the beam is narrower in the horizontal x-direction parallel to the electric field and wider in the vertical direction. Fig. 5(b) shows the appropriate cross section along the x- and y-axis in two dotted curves. For comparison a Gaussian beam with circular symmetry and equal total power is fitted to the soliton solution and illustrated by the solid line. As required by the ansatz, the elliptically shaped soliton solution remains entirely unaltered when it propagates through the crystal.

In contrast, a numerical beam propagation starting from a Gaussian beam depicted by the solid curve in Fig. 5(b), shows strong oscillations of its shape. Both transverse diameters

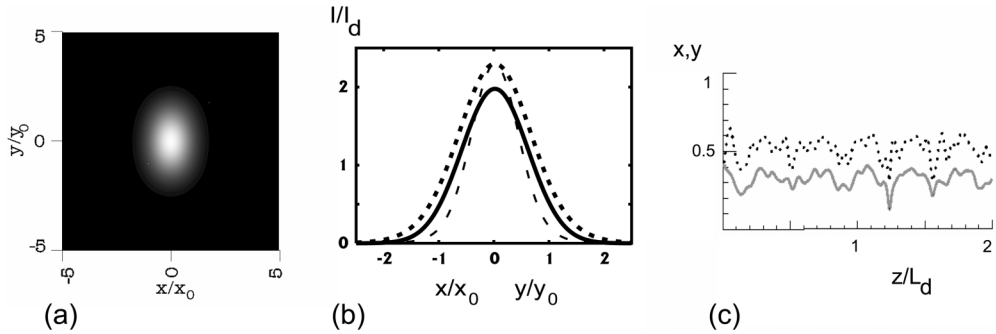

Fig. 5 (a) Two dimensional contour plot of a soliton solution in anisotropic medium. (b) Cross sections along x-axis (dashed) and y-axis(dotted) in comparison with a fitted Gaussian beam of equal total power (solid). Evolution of a diameter of a Gaussian beam at the intensity of $I/I_d = 1.5$ accompanied by oscillations of its diameter in x(solid) and y(dotted) (Petviashvili-based simulation by K. Motzek, TU Darmstadt)

oscillate. As a consequence, the beam shape varies from almost circular symmetric to strong elliptical which is depicted in Fig. 5(c) for a distance of 7.2 cm in real units. It has been shown by Zozulya et al. [50] that the ellipticity of the soliton solutions depends strongly on the beam intensity and hence on the saturation parameter I_d.

As the normalized intensity $I = I_{\mathrm{beam}}/I_d$ approaches zero, the diameters $d_{x,y}$ at half maximum are inversely proportional to the square root of the intensity, $d_{x,y} \propto 1/\sqrt{I}$. In the high-intensity limit they obey $d_{x,y} \propto \sqrt{ln(I)}$. For $I > 50$, the oscillatory behavior becomes very strong and reaches about 25% of the peak intensity. In the intermediate saturation regime ($I \approx 1 - 10$), the fluctuations become reasonably damped and the self-focused beam almost converges into the exact soliton solution. An optimized damping exists when the ratio of beam to background intensity $I \approx 0.5$ [50,51]. In this case the oscillations are smaller than 5% and the usage of the expression "soliton" is indeed justified. For a stable photorefractive soliton the diameter ratio is $d_x/d_y \approx 1/1.5$.

Whereas theoretical studies explained the anisotropic shape of photorefractive screening solitons, the first experimental results were somehow contradictory. In [52,53] a self-focused light structure of a radially symmetric shape was observed. Such a behavior can be explained due to the fact that the solitary beam is in a transient state at the experimental observation plane. Meanwhile, it is commonly accepted that photorefractive screening solitons are indeed anisotropic and display an elliptical transverse shape [54].

The self-focusing effect originates only from the drift of the photo-excited electrons in the crystal. Figs. 3–4 illustrate that already the drift-induced refractive index modulation is inherently anisotropic. Omitting the diffusion of electrons does not affect the refractive index modulation and the formation of a photorefractive soliton in principle, but it is essential for a full description of the physical processes that take place in the bulk medium. As already mentioned and depicted in Fig. 2(h), the general influence of diffusion leads to a transverse deflection of the beam during propagation [44]. This effect, which is a by-product of soliton generation, has been predicted [45,47,51,55] as well as investigated experimentally [56,57]. The bending effect takes place when the circumference of the light intensity distribution becomes comparable to

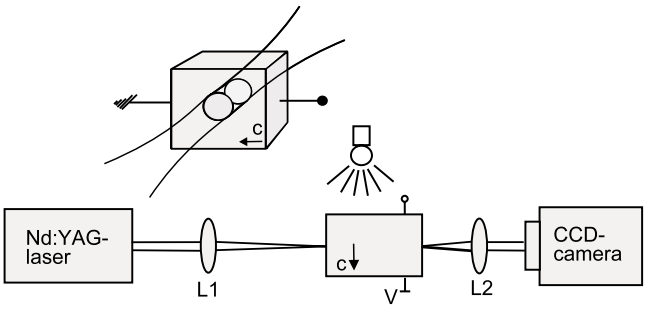

Fig. 6 Sketch of the experimental setup. The inset on top shows the crystals geometry from a front view

the diffusion length of the free electrons in the material. Therefore it will be observed when the light beam is already tightly focused. In our further investigations it should be taken into account that the generation of photorefractive screening solitons always comes along with self-bending of the soliton trajectory. Nevertheless, this has no direct influence on the self-focusing effect itself. It only gives rise to a transverse shift of the beam towards the external electric field.

3.4.2 Experiment

To generate screening solitons in a photorefractive crystal, the material has to fulfill several distinct requirements. For the generation of a light-induced focusing refractive index modulation the charge carrier migration has to be drift-dominated (compare i.e. Fig. 2) and the net refractive index change Δn which is given by Eq. (9) has to be in the range of 10^{-4} to compensate the diffraction of the light beam. Taking these requirements into account, Strontium Barium Niobate – SBN – is an ideal candidate for the generation of spatial (2+1)-dimensional soliton, having a $4mm$ symmetry. When an external electric field is applied along the crystalline c-axis and the incident light is extraordinarily polarized (parallel to the c-axis) the effective electrooptic effect r_{eff} almost equals the relatively large r_{33} electro-optics coefficient of SBN, which is in the range of $200 - 1400$ pm/V depending on the specific dopant concentration and crystal constitution.

Fig. 6 shows a sketch of the relatively simple experimental setup, which uses an extraordinarily polarized light beam at $\lambda = 532$ nm derived from a frequency-doubled Nd:YAG-laser. The lens L1 focuses the beam onto the front face of the SBN crystal, where it has a minimum beam waist of $15\ \mu\text{m} - 20\ \mu\text{m}$ at the full width at half maximum (FWHM). We make use of three different crystal samples that have the same transverse dimensions of $5 \times 5\ \text{mm}^2$ but are different in length, ranging from 10 mm via 13.5 mm up to 20 mm. Finally, the exit face of the crystal is monitored with the help of lens L2 onto a CCD-camera allowing computer-aided acquisition of the evolving light structure. In case of zero applied voltage the material acts as a linear medium with a refractive index of $n_e = 2.3$, and we are able to monitor the incident light intensity. Depending on the beam's incident size and length of the specific sample, the propagation distance within in the crystal represents 3.5 to 5 diffraction lengths.

By applying a dc-voltage along the crystallographic c-axis of 2–4 kV/cm, the charge carrier transport becomes drift-dominated and the material acts highly nonlinear. Because it is impossible to observe any structure within the bulk material, we are restricted to observe the exit face of the crystal. Additional, the SBN crystal is illuminated homogeneously with incoherent white light that corresponds to the dark intensity I_d. Thereby, we have an effective tool on

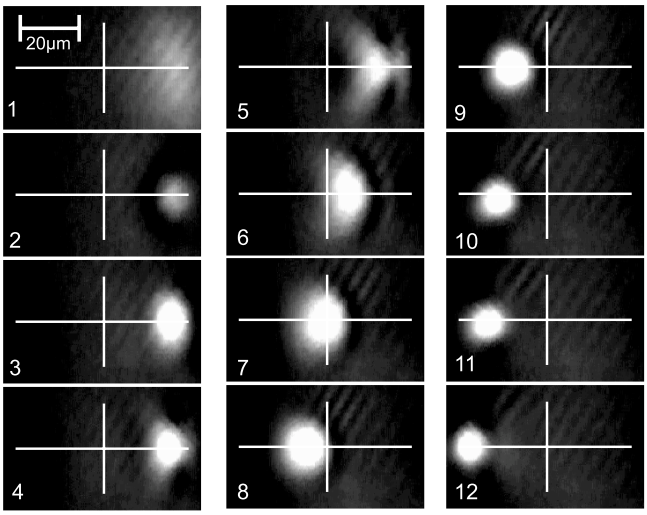

Fig. 7 Temporal sequence of soliton generation. The single frames (1–12) are taken every 0.5 s after the shutter has been opened. First of all the beam experiences a strong focusing (1–4) before the diffusion effect comes into play at fairly small beam diameters, resulting in a horizontal displacement (5–12)

hand to manipulate the dark and thermal conductivity of the electrons in the material. In all our experiments we make sure that the ratio of dark- to beam intensity is in the range of unity to achieve stable solitons.

The beam intensity is in the range of a few Microwatts, whereas the white light intensity is measured in a separate experiment via two beam coupling. When all parameters are within the soliton existence range, self-focusing takes place and diffraction can be completely balanced. Finally, the initially Gaussian beam of circular geometry evolves into an elliptically shaped photorefractive soliton without significantly changing its transverse size.

The dynamic generation process of a photorefractive screening soliton monitored from the exit face of the crystal is illustrated in Fig. 7 in a temporally-resolved sequence. Before opening the shutter, the white light illumination is in the range of the total beam power of 1.85 µW and the bias electric field is 3.8 kV/cm. In the first second after the shutter opens, the material does not yet respond to the incident light beam which diffracts almost linearly. After about 0.5 s the photo-induced space charge field becomes large enough to modify the refractive index significantly. As a consequence, the beam starts to self-focus (compare to Fig. 7(#2–#4)). Once the beam is tightly focused the influence of the diffusion-driven electron transport grows and the beam undergoes a transient re-shaping process while it deflects about 60 µm in the direction of the applied electric field (Figs. 7(#5–#11)). About 7 seconds after opening the shutter, the soliton reaches a steady state and displays its typical elliptic shape in Fig. 7(#12). The figure clearly shows that the diffusion process only becomes important when the light structure is tightly focused [58]. Therefore, self-focusing is solely a result of a drift-dominated redistribution process.

A reasonable effect of self-focusing of light exists within a fairly large range of parameters around the exact soliton solutions given by the theory [47, 50, 51]. Therefore, it is a quite easy task to generate stable self-focusing in a SBN crystal with a beam of Gaussian intensity distribution. Nevertheless, it is still an open challenge to resolve any oscillations of the beam profile along the propagation direction. The material is highly non-linear and a technique of imaging through the crystal can not be applied [40, 59]. There have been basically two

approaches to study the spatial evolution of photorefractive solitons. The first one [52] makes use of a top-view photograph immediately after the background beam has been blocked. For larger beam diameters, it shows nicely the formation of a solitary structure but the spatial resolution is too poor and only one of both transverse profiles can be investigated. The second method is based on a specially cut crystal [52]. Its exit face is not normal to the c-axis but cut at a certain angle. By laterally shifting the input beam the authors of [52] were able to investigate different propagation lengths. One has to take into account that all experimental approaches bear the insufficiency of the sample due to inherent inhomogeneities of the material. Additionally, the applied electric field cannot be estimated to be entirely uniform throughout the bulk material, and the shape of the incident light beam is Gaussian and not of a required soliton type. Taking these aspects into account we developed a third method that is based on the exploitation of the dynamical behavior. From the response of slight variations of the external parameters, one can draw all conclusions whether the observed self-focusing represents a soliton solution or not: a soliton solution should be quite robust and withstand slight disturbances within the system. In contrast, strong dynamical fluctuations are an indication that the system operates outside the soliton existence range.

4 Interaction of scalar solitons

Solitons are not only characterized by their self-confinement in time or space. Several of their most peculiar and specific features display in their particle-like interaction behavior [60]. Therefore, interaction studies are essential for a complete characterization of solitons. In (1+1)-dimensional Kerr systems, the interaction of two single solitons is limited to a two-dimensional plane. But since the system is integrable, a collision between single solitons is fully *elastic*, which means that the number of solitons is conserved and that the single solitons recover their initial trajectory and shape after the collision [61]. Investigating spatial soliton collisions in the bulk material gives rise to a variety of new and fascinating effects since the system is not restricted to one single collision plane anymore. However, we have to take into account that stable self-trapping in both transverse dimensions is only possible if the nonlinearity of the medium is of a saturable type at the expense that the system is no longer integrable. Therefore, collisions are accompanied by radiation losses. As a consequence, the number of solitons may not be conserved anymore and the shape of the beams may become strongly affected. In general, collisions of solitary waves in a saturable nonlinear medium can be characterized as *inelastic* since the collision progress comes along with energy dissipation, and the single particle-like waves do not necessarily maintain their profile or identity. Since saturable media support the formation of solitary beams in a bulk material, interaction scenarios can now be studied in all three spatial dimensions. This gives rise to new and fascinating effects such as fusion, fission, or mutual attraction and repulsion of solitons.

Among these different kinds of scenarios one has to classify between *coherent* and *incoherent* interactions. In coherent systems, the two (or more) solitons are mutually coherent and naturally there exists some kind of interference pattern in their intersection region. When the response time of the material is short and within the range of the interference fluctuations, the interaction is said to be coherent, since the material responds to the interference pattern of the two intersecting beams. In this case the resulting refractive index modulation corresponds to the superposition of two (or more) beam amplitudes. In contrast, when the response time of

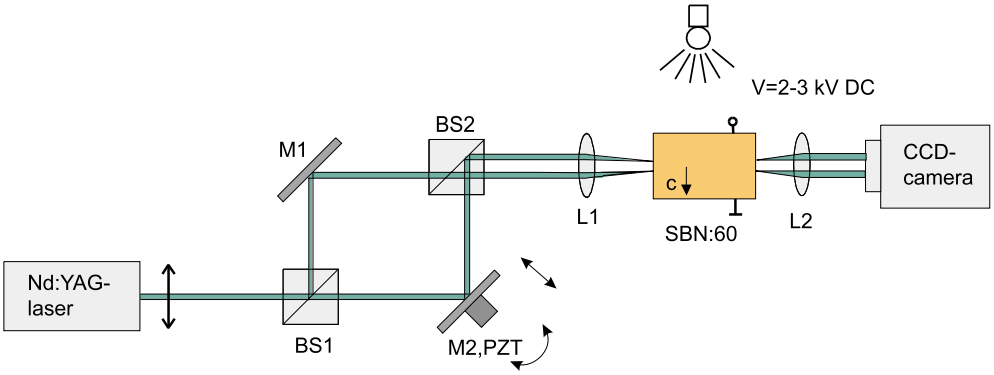

Fig. 8 Schematic configuration of incoherent soliton interaction. BS: beam splitters, M_1, M_2: mirrors, L_1, L_2: lenses, PZT: piezoelectric transducer, V: externally applied voltage

the material is non-instantaneous, as e.g. for all photorefractive systems, coherent interactions can only be realized when the interference pattern of the intersecting beams is stationary in time. In contrast to that, an interaction is said to be incoherent when the phase fluctuations of the interacting components are much faster than the response time of the material. In this case, the nonlinear index change is only due to a superposition of the intensity of the single beams, and they appear to be mutually incoherent.

To investigate interactions in the full three-dimensional geometry we make use of the experimental setup depicted in Fig. 8. In contrast to the experimental setup for the generation of a single soliton, we now derive two beams using a Mach-Zehnder-like configuration realized by the mirrors M1, M2 and two beamsplitters BS1, BS2. In order to investigate coherent as well as incoherent interactions, mirror M2 is connected to a piezoelectric transducer (PZT) which may either shift the phase of one beam relative to the other or may oscillate at a frequency of about one kHz, thereby inducing a rapidly oscillating interference pattern when the two beams recombine in the crystal. The latter scenario makes the two beams effectively incoherent with respect to each other. Moreover, with the help of the two mirrors, the beams can be aligned in every desired direction and position. To reveal a certain interaction effect, we always compare the position of the single beams in case of separate with simultaneous propagation. Due to the slow response of the crystal we are even able to identify the single beams by blocking one of them and recording immediately the resulting intensity distribution of the remaining light beam at the exit face of the crystal.

4.1 Interaction of coherent solitons

To investigate coherent interactions of spatial solitons in a (2+1)-dimensional photorefractive system, the interference pattern of the two light beams has to be temporarily stationary, since the crystal has a rather slow response time. As will be demonstrated below, the main control parameter of coherent interactions is the relative phase of the interacting beams, which therefore has to be kept constant. Suppose we have two mutually coherent light beams of Gaussian shape incident in a parallel way on a photorefractive crystal. The trajectories run within a x-z-plane and keep a constant distance which is comparable to their transverse diameter. In Fig. 9 we

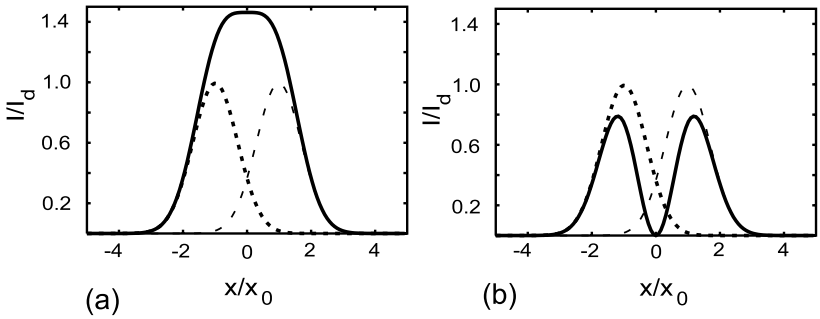

Fig. 9 (a) Separate illustration of the intensity distribution of two coherent overlapping beams (dotted curves). Resulting interference pattern for a relative phase difference of $\varphi = 0$ (a) and $\varphi = \pi$ (b) (solid lines)

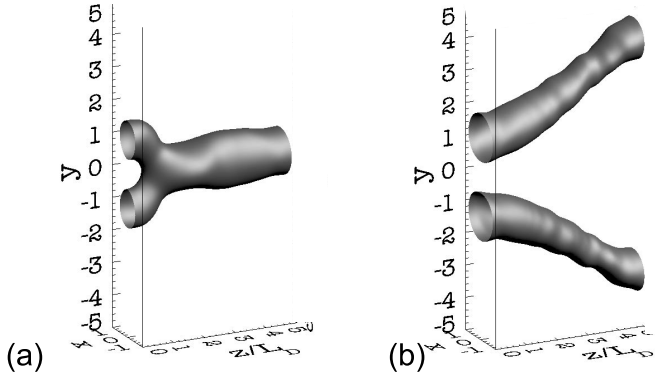

Fig. 10 Propagation dynamics of two coherent Gaussian beams in an isotropic saturable nonlinear medium visualized by an isosurface-plot for $I = 80\%$ of the soliton's initial peak intensity. Depending on their relative phase, the beams attract ($\Delta\varphi = 0$) (a), or repel ($\Delta\varphi = \pi$) (b)

illustrate the influence of the mutual phase on the net intensity distribution which induces the refractive index modulation. The two slightly overlapping coherent beams are depicted as dotted curves in Figs. 9(a),(b), and the resulting interference pattern is illustrated by the solid line. In Fig. 9(a) the two beams are in phase ($\Delta\varphi = 0$) and the net intensity in their central region increases remarkably. From our previous investigations it is clear that a non-zero light intensity induces a refractive index elevation that acts in a self-focusing way. As a consequence, light will be attracted towards the central region and the solitons appear to attract each other. We now suppose that the beams are out of phase ($\Delta\varphi = \pi$), which is depicted by Fig. 9(b). The destructive interference leads to a region of zero intensity in between the two beams. Now, the opposite effect takes place. The intensity in the center of the two solitons is lower than it would have been if the beams were further apart. Consequently the beam centers move away from each other with increasing propagation distance and the solitons appear to repel each other.

In Fig. 10 we present the typical propagation dynamics of two parallely launched coherent solitons in an isotropic saturable medium. The three-dimensional visualization represents an iso-surface of the propagating beams at 80% of the normalized beam intensity.

Fig. 10(a) illustrates a side-view when the relative phase between the beams is zero and the two beams merge after one diffraction length and form a multi-mode waveguide. The scenario

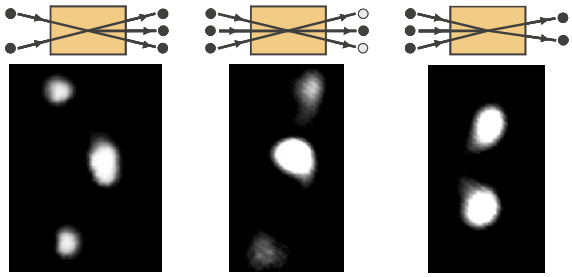

Fig. 11 Creation and annihilation of photorefractive screening solitons due to multi-soliton collision. (a)-(c) illustrate the exit face if the crystal and the sketches on top depict the solitons propagation through the crystal. Frames taken from [32]

changes dramatically when the beams are out-of phase, which is depicted in Fig. 10(b). The two solitons repel strongly and their initial separation of 2.3 increases to 7.2 after a propagation of 5 diffraction lengths.

Interaction scenarios in (2+1)-dimensional saturable systems are not limited to the relatively simple effects of mutual repulsion and attraction for parallel propagating solitons, but show an even more complicated behavior. In 1992 Gatz and Herrmann [62] demonstrated numerically that two coherent in-phase solitons can fuse in a (2+1)-D saturable system when they intersect at a shallow angle. Later on, Snyder and Sheppard [26] demonstrated theoretically that coherent solitons can even undergo a fission process that gives *birth* to an additional solitary beam. Both scenarios have also been verified experimentally. The fusion process is universal for all saturable nonlinear systems, and has been observed in liquids [63], glass waveguides [61], atomic vapours [27, 64] and in photorefractive crystals [29, 65, 66]. With the help of a simple waveguiding model [26] these effects can sufficiently be explained. Both beams propagate in a self-induced waveguide that is characterized by a critical angle $\alpha_{\mathrm{crit}} \approx (n_{\mathrm{max}} - n_{\mathrm{min}})/n_{\mathrm{max}}$ for guidance. Here, α_{crit} characterizes the maximum angle up to which total internal reflection and thus waveguiding occurs. When the intersection angle of two coherent beams is below α_{crit} they couple light into each others waveguide and exchange energy. Because of the attractive interaction, the two beams merge and form a joint multi-mode waveguide in which they both propagate. In case the intersection angle exceeds the critical angle, the two beams just intersect each other and remain almost unaffected. In [29] α_{crit} was determined experimentally to $\alpha_{\mathrm{crit}} = 0.6^\circ$ and merging of two single solitons has been observed. In a similar experimental arrangement Królikowski et al. [31] increased the intersection angle slightly to $\alpha \approx 0.8^\circ$ and observed the generation of an additional beam that was generated upon collision. Moreover, the annihilation of one soliton via a multi-soliton collision process [32] was demonstrated. This unique feature of photorefractive screening solitons is depicted in Fig. 11. The sketches on top of each frame depict the geometry of the intersecting beams, whereas the single pictures display the exit face of the crystal. In order to avoid photorefractive two-wave mixing that takes place along the crystallographic c-axis, the intersection is carried out in the vertical y-z-plane. Fig. 11(a) shows the *birth* of a soliton that results from two intersecting beams. Since the centrally located created soliton is stronger in intensity than the two non-central beams, it experiences a stronger bending effect which results in a lateral displacement. In Fig. 11(b) the opposite effect takes place. Launching three beams at a slightly different intersection angle into the crystal results in a transfer of energy from the outer solitons towards the central one. In this way, a single soliton can be amplified. Fig. 11(c) finally illustrates the complete annihilation of

the central soliton. In this way it becomes clear that in (2+1)-dimensional systems solitons can be created as well as annihilated through coherent interaction processes. Even though these effects may serve as principle tools for optically controllable waveguide interconnects, they are strongly dependent on the relative phase of the single beams, which has to be kept constant throughout the interaction. Because of this strong phase sensitivity, the realization of technical applications that have to withstand strong perturbations is almost unapproachable. Therefore, our further investigations focus on interaction of mutually incoherent beams.

4.2 Interaction of incoherent solitons

In contrast to coherent interactions, the optical fields of mutually incoherent solitons do not produce any interference pattern. The resulting intensity which affects the material is equal to the superposition of the intensity of the two single components. We like to emphasize that in this context the expression *incoherent interaction* has to be interpreted as the interaction process of two coherent light beams that are mutually incoherent. Their relative phase fluctuates much faster than the response time of the nonlinear material. Therefore, the material responds only on a time averaged intensity pattern and the beams appear to be mutually incoherent. Since destructive interference as depicted in 9(c) is absent, any two mutually incoherent beams do always attract but never repel in saturable nonlinear media. As well as in the coherent case, two solitons can fuse if the relative angle is below the critical angle α_{crit} [29]. Pure phase-dependent effects such as soliton fission or annihilation that were observed in coherent systems shall not occur with mutually incoherent beams. From the practical point of view, interactions of mutually incoherent solitons are very robust, since the effect of attraction is not phase sensitive. This unique property motivates further investigations of interaction studies. A potential application of re-configurable waveguide interconnects may be realized on the basis of spatial soliton interactions [26, 67–71].

4.2.1 Anomalous interaction in anisotropic media

The first investigations on incoherent interactions of screening solitons in a photorefractive crystal [29] demonstrated indeed fusion and mutual intersection of solitons depending on their collision angle. However, the anisotropic refractive index modulation of a photorefractive SBN crystal bears a unique property that reveals a supplementary and surprising incoherent interaction process. It is denoted as *anomalous interaction* and has been investigated experimentally and numerically in [30]. Depending on their relative distance and orientation, mutually incoherent solitons do not always attract but can even repel as they propagate through the crystal. Therefore, photorefractive solitons have become a promising tool to realize various interaction scenarios that display both essential effects – repulsion and attraction – on the basis of mutually incoherent optical beams.

Suppose we have two mutually incoherent beams of Gaussian shape launched in parallel into the x-z-plane of a photorefractive SBN crystal. In contrast to coherent interaction, the beams do not interfere but each single beam itself induces a nonlocal refractive index modulation as depicted in Fig. 3. In Fig. 12 we demonstrate how the refractive index modulation (bottom row) evolves for two different horizontal separations of the beams (top row). Due to the nonlocal response of the material, the refractive index modulation that is due to the optically-induced space charge field, covers a larger area than the optical field itself. Therefore, the single space charge fields and hence the refractive index modulations of two closely propagating beams

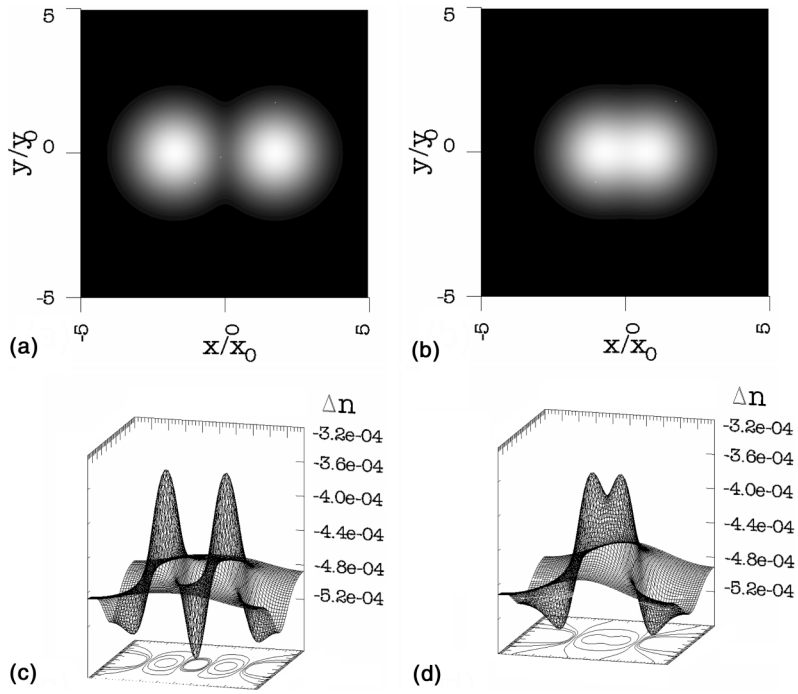

Fig. 12 Intensity distribution of two mutually incoherent Gaussian beams (a),(b) and the corresponding refractive index modulation Δn for various horizontal separations of $\Delta x = 1.7$(a),(c), $\Delta x = 3.5$(b),(d)

superimpose. In Fig. 12(a) the separation of the beams is in the range of their diameter, the optical fields do not overlap, but the induced space charge fields superimpose and form a joint refractive index modulation which is illustrated in Fig. 12(c). Since the refractive index decreases at the beam's horizontal edges, the net refractive index change between the two solitons becomes negative. Despite the fact of a non-zero intensity in the intersection region and the lack of destructive interference, the solitons will repel as they propagate through the crystal. When the separation of the beams is decreased further (Fig. 12(b)), the optical fields start to overlap, and hence the net refractive index change depicted in Fig. 12(d) between the two solitons becomes positive and the interaction will be attractive. In order to demonstrate this remarkable behavior in experiments, we align two beams in the plane parallel to the electric field at various horizontal distances and record the resulting images that appear at the exit face of the material. The mutual interaction of the two solitons is illustrated in Fig. 13. The independently propagating beams are illustrated versus a coupled and hence simultaneous propagation in the upper and bottom row of Fig. 13, respectively. The frames that display the non-interacting behavior (Fig. 13(a)–(c)) were obtained by allowing each beam to propagate separately in the crystal and by superimposing the resulting images subsequently. We realized three different configurations with varying lateral separations. Fig. 13(a) illustrates two closely propagating non-interacting solitons that are separated by $13\ \mu\mathrm{m}$ and their corresponding interaction in Fig. 13(d). It is obvious that the two beams fuse as they interact and leave the crystal as

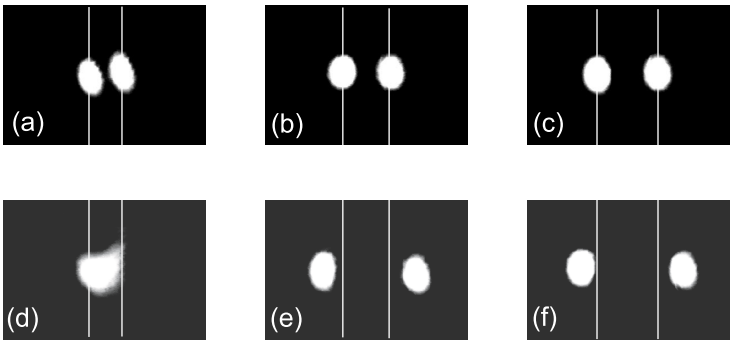

Fig. 13 Experimental realization of separation-dependent interaction of incoherent solitons. The upper row shows non-interacting solitons for various separations of $\Delta x = 16$ μm(a), 25 μm (b) and 33 μm (c), and their corresponding attractive (d), or repulsive interaction (e), (f), respectively

a single solitary beam. This behavior is essentially the same as that for overlapping beams in an isotropic saturable Kerr-like medium [24]. In Fig. 13(b) we slightly increase the lateral separation to 25 μm and the appropriate interaction depicted in Fig. 13(e) displays a remarkable repulsive effect. After propagating 13.5 mm through the crystal, the relative distance increases roughly to 50 μm. When we further increase the initial separation up to 33 μm in Fig. 13(c) the repulsive effect is still present but reduced (compare Fig. 13(f)). Although the optical fields hardly overlap in all depicted scenarios, the interaction behavior depends strongly on the mutual separation of the two solitons. This soliton interaction effect is unique for spatial solitons, displaying especially the nonlocal material response of a photorefractive crystal. We like to emphasize here, that the experimentally obtained results are in a very good agreement with numerical simulation based on the anisotropic model [30, 58, 72].

To characterize the anisotropic refractive index modulation more specific, we also investigate interaction effects in the direction perpendicular to the externally applied field. In the transverse y-direction the refractive index modulation increases over the entire transverse cross-section of the beam (compare Fig. 4(d)). Therefore, from any superpostition of two mutually incoherent beams in the z-y-plane, no negative index modulation can evolve and the solitary beams will never experience any repulsive effect.

With the same technique as described above we illustrate in Fig. 14 the exit face of the crystal in the case of non-interacting beams in the top row (Fig. 14(a)–(c)) and the corresponding interaction images underneath (Fig. 14(d)–(f)). The experimental parameters are nearly unchanged compared to the interaction scenario in the horizontal plane which is depicted in Fig. 13. For a small separation of the beams of 15 μm (Fig. 14(a)), the strong attractive force causes the trajectories of both solitons to intersect (Fig. 14(d)), which results in an oscillating behavior, that leads to an exchange of the soliton's position at the exit face. For a larger distance of 30 μm, the attractive force weakens and leads to a much longer propagation distance until the solitons collide (Fig. 14(e)). In this particular case the solitons merge very close to the observation plane at the end of the crystal. For an even larger initial separation of 50 μm (Fig. 14(c)) only a significantly weaker attraction can be observed which results in a slightly decreased separation at the exit face (Fig. 14(f)). The isosurface plots in Figs. 14(g),(h) depict the trajectories of the

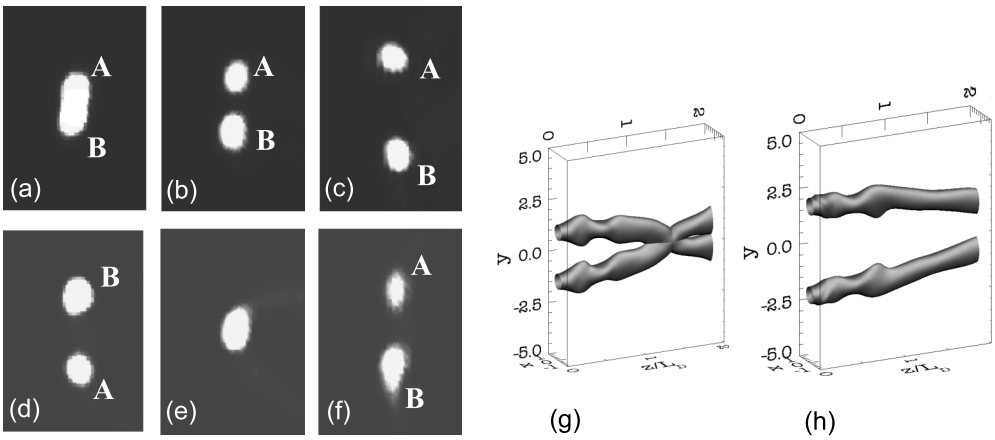

Fig. 14 Experimental (a)–(f) and numerical (g)–(h) results of attraction of incoherent solitons in the vertical direction. Separate and coupled propagation for a separation of 15 µm (a),(d), 30 µm (b)(e), and 50 µm (c)(f). Frames taken from [58]

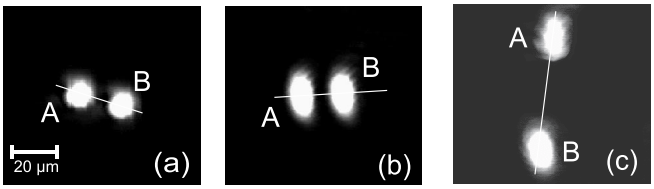

Fig. 15 Three-dimensional interaction. (a) incident beams, (b) non-interacting solitons at crystal's exit face, and (c) the corresponding interacting scenario that displays a rotation of about 90°

beams at 80% of the initial peak intensity for an initial separation $d_y/y_0 = 2.4$ in Fig. 14(g) and $d_y/y_0 = 4.0$ in Fig. 14(h). As already demonstrated in the experiment, the attraction increases with decreasing initial separation, and the beams even intersect each other.

In general, our numerical results are in a good agreement with the experimentally observed phenomena. The movement and the intersection in particular can be interpreted on the background of an induced transverse momentum which is due to the mutual attraction. The particle-like waves accumulate a *transverse momentum* as they mutually approach. When they finally collide, their collision angle is above the critical angle of the self-induced waveguides. Consequently, the solitons do not merge but intersect and their transverse separation increases again. Since they still attract each other, the whole process repeats several times leading to a periodic collision of solitons. Because the system is of a self-focusing saturable type, the amplitude of these transverse oscillations is damped and the solitons might coalesce at very large propagation distances [58].

In contrast to a propagation of the solitons within the plane parallel to the externally applied field, the interaction in the perpendicular direction is always attractive. Since both effects, mutual repulsion as well as attraction depend on the orientation and on the separation of the single solitons, a superposition of these effects by means of tilting the propagation plane with respect to the x-axis gives rise to three-dimensional interaction processes, that are subject of the next section.

4.2.2 Three-dimensional interaction scenarios

Due to the anisotropic refractive index modulation there exist attractive or repulsive domains, depending on the position and separation of the single solitons. This remarkable characteristics is well-suited to study interaction effects of an elaborated geometry. The simultaneous interplay of attraction and repulsion leads to rotational effects that are studied in detail in [58, 72]. In Fig. 15 we present the experimental result of such a rotational interaction when two beams are launched almost in parallel but tilted with respect to the x-axis. In this way they experience attraction along the y-axis but repulsion along the x-axis. Fig. 15(a) illustrat'es two Gaussian beams of circular symmetry that are incident on the SBN crystal. Beam A is horizontally but also slightly vertically shifted relative to beam B. When each beam itself propagates in the biased crystal and forms an elliptically shaped photorefractive soliton, they end up in a horizontal plane at the exit face of the crystal, which is indicated by the horizontal line in Fig. 15(b). This image displays again a superposition when each soliton propagates separately. When the two beams finally propagate simultaneously, the position of both solitons becomes strongly affected and their propagation plane rotates about $90°$. Additionally, their absolute separation increases remarkably as shown in Fig. 15. This behavior is only due to the anisotropic refractive index modulation. Numerical studies [58] on the basis of the anisotropic model reveal the same effect in good agreement with the experimental data.

Since the solitons rotate remarkably as they propagate simultaneously in this configuration with a negligible initial transverse momentum, it is of huge interest to investigate interaction effects when both beams are propagating with non-parallel, but skewed trajectories. In the early nineties it has already been demonstrated numerically that rotational effects can occur in isotropic saturable nonlinear media [73, 74] if the beams are launched with skewed trajectories. It has been predicted that spatial solitons can even fulfill a spiraling helix-like motion when the divergence of the trajectories is counterbalanced by their mutual attraction. This is certainly the case in an isotropic medium whereas photorefractive crystals may not support such a continuous motion due to their inherent anisotropy.

With the help of the experimental configuration depicted in Fig. 8, Shih et al. [75] report on the observation of a continuous spiraling motion of photorefractive solitons. This is a quite involved task because it is generally not possible to follow the beam trajectories inside the crystal experimentally. Since the medium is highly nonlinear one cannot simply record various transverse planes inside the crystal. Experimentalists are therefore always restricted to an observation of the crystal's exit face. To investigate at least two different observation planes, Shih et al. flipped the SBN crystal in such a way that the beams propagated either along the crystallographic a- or b-axis that were different in length for the given crystal sample. Comparing the resulting images at the three different stages of propagation, they concluded that the two solitons perform a continuous rotation of about $540°$, but were not able to give a final proof. In a subsequent publication [76], the authors tried a different experimental approach by recording a series of output images while keeping the relative angles of the beams constant but modifying their initial separation. The beams are launched at a fairly large lateral distance into the crystal in a way that they start to interact after a certain propagation distance. When only the initial lateral displacement is decreased, the interaction region moves toward the front face of the crystal and the effective spiralling path – the distance between the interaction region and the exit face – becomes larger. Now, Shih et al. were able to observe a rotational motion as

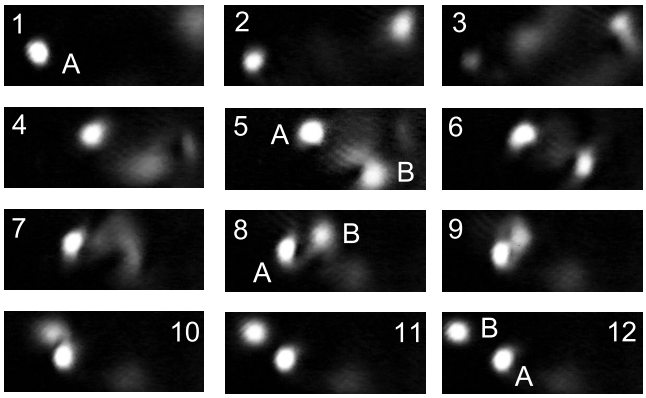

Fig. 16 Time-resolved complex rotation of a soliton pair. The single frames (1)–(12) show the crystal output immediately when the second beam is launched. The time interval between successive frames is 0.36 s

they modify the initial separation of the beams and interpreted that the two soliton trajectories describe a spiraling path as they propagate through the medium.

In order to reveal the nature of this complex propagation scenario, we implemented a novel, third approach that is based on the formation dynamics of photorefractive solitons. Two appropriately aligned beams are launched subsequently into the crystal. Fig. 16 illustrates a temporal sequence when the first beam A has already formed a soliton and the second beam B is just launched into the crystal. Comparing frames (#1) and (#5) of Fig. 16, one can detect a clockwise rotation of about 60° of the soliton's propagation plane. Whereas in the subsequent frames of Fig. 16(#6–#12) a counter-clockwise motion of about 180° can be observed. This sequence gives a clear indication that the two beams propagate along spiraling or at least twisting trajectories through the nonlinear medium. The question if photorefractive screening soliton are, under special circumstances, really capable of fulfilling a spiraling and not only a twisting motion can finally not sufficiently answered from the experimental results. However, numerous numerical studies [77,78] demonstrate clearly the impact of the anisotropy on such a spiraling motion. They revealed that the optical beams have to be launched in a special skewed way to propagate as spiraling solitons, otherwise the inherent anisotropy prevents the solitons from spiraling around each other and creates an oscillatory and twisting motion as the beams propagate in the material.

5 Wave guiding in photorefractive solitons – "light is guiding light"

Because every phenomenon of confined light propagation can be interpreted by means of linear waveguide theory [79], the special case of self-trapped optical beams can be explained by means of the so-called self-consistency principle (see e.g. 2.4 and [33,34]). In this model, an incident light beam induces a refractive index waveguide which is capable of guiding the beam itself as an eigenmode. Moreover, (1+1)D Kerr-type spatial solitons are not only able to guide their basic induced mode but also other beams due to cross-phase modulation effects [80,81]. Therefore, a single beam basically creates a waveguiding structure in which other beams of different power, wavelength or transverse geometry can be guided. This optical control of one beam by another one bears an immense potential for applications in all-optical switching and waveguide-coupling purposes.

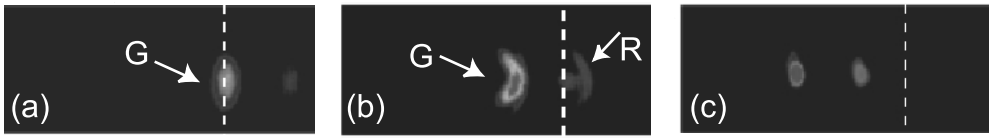

Fig. 17 Dynamics of soliton formation of a beam at $\lambda = 532$ nm (G) when guiding a probe beam at $\lambda = 633$ nm (R). The probe beam is located at the right side of the soliton due to a spatial frequency selection by using a prism in front of the recording CCD camera. The time interval between consecutive frames (a)–(c) is $\Delta t = 3s$)

Due to these generic and obviously promising features of nonlinear spatial solitons in linear optics, investigations of the waveguide characteristics of self-trapped optical beams in saturable photorefractive media suggest themselves. Moreover, a helpful feature that facilitates the realization of waveguide structures is the strong wavelength dependence of the photorefractive effect. Therefore, it is possible to derive a soliton from a weak incident beam and guide a much stronger beam of a different wavelength for which the material is much less photosensitive. Consequently, waveguiding has been observed soon after the experimental realization of photorefractive solitons for quasi-steady-state solitons [82], and subsequently for stable screening photorefractive solitons [69, 71, 83].

5.1 Photorefractive waveguides

Exploiting the wavelength selectivity of the photorefractive effect, Shih et al. [69] demonstrated guiding of a 15 μW He-Ne-laser ($\lambda = 633$ nm) probe beam in a soliton, which was induced by a ten times weaker writing beam of 1.5 μW,($\lambda = 488\ nm$) derived from an Ar^+-laser. In the absence of the writing beam $\lambda = 488$ nm, the probe beam of $\lambda = 633$ nm diffracts linearly in the biased crystal and does not form a self-confined structure. Only when the writing beam is present, the refractive index of the material changes, the required waveguide is induced, and the probe beam is trapped in the soliton. The coupling efficiency of the red beam into the soliton waveguide could be determined to be 85%, normalized to the absorption of the material ($\alpha = 0.21$). If the dark conductivity of the material is low, the refractive index channel formed by the photorefractive soliton can even be persistent enough to guide other beams without being present. In our experimental investigations, we were able to use such a waveguide structure for guiding purposes of a beam at $\lambda = 633$ nm for several days without significant degradation of the waveguide structure [71]. For details on fixing photorefractice solitons see e.g. [84]. Fig. 17 shows the formation of such a waveguide at $\lambda = 532\ nm$ and the guiding of a probe beam of $\lambda = 633$ nm. Both beams have an intensity of about 30 μW and propagate in a 13.5 mm long SBN crystal. During the formation of the soliton waveguide channel, the effects of self-focusing, which is accompanied by beam diameter oscillations and beam bending effects can clearly be identified in the soliton G as well as in the guided beam R. Note that in steady state (Fig. 17(c)), the typical anisotropic nature of the waveguide also defines the shape of the guided beam.

Generic multi-mode waveguides are not only capable of guiding modes with a different wavelength, but also with a different and more complex geometry. In contrast to Kerr media, where only relatively weak beams can be guided by a soliton, the saturable nonlinearity supports

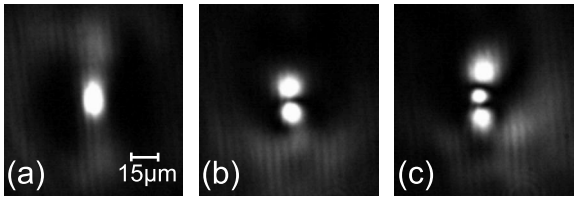

Fig. 18 Excitation of ground- and higher-order waveguide modes with a red probe beam. (a) fundamental mode TEM_{00}, and the higher-order modes TEM_{01} (b), and TEM_{02} (c)

the realization of multi-mode soliton-induced waveguides, where the probe beam can even be much stronger than the guiding beam. Due to the fact that the number of supported waveguide modes is directly proportional to the degree of saturation, it increases with increasing ratio of beam to background intensity. In the regime of moderate saturation, which corresponds to the region of the two-dimensional soliton solution, only a limited number of modes can be excited, moreover reflecting the anisotropic nature of the photorefractive soliton.

Therefore, guiding of a double- or triple-humped transverse light structure resembling TEM_{01} and TEM_{20} transverse laser modes has successfully been demonstrated in both transverse directions for the case of high saturation (where the background intensity was 120 times stronger than the waveguide-inducing structure) [69, 85]. However, in this case, the transverse structure formed by the nonlinear refractive index change is no longer close to the soliton solution, thereby demonstrating that a stable solitary beam formation is not obligatory for waveguiding purposes.

In a recent numerical and experimental study [83] that emphasizes the anisotropic nature of the refractive index modulation and hence the self-induced waveguide structure, the waveguiding features have been exploited to visualize the anisotropic refractive index modulation of the photorefractive nonlinearity. Using a soliton-induced waveguide with a size of about $15\ \mu$m in diameter, a probe beam enlarged to a diameter of $100\ \mu$m was used to scan the entire transverse structure of the waveguide. Since the probe beam is much wider than the solitary structure, only part of the incident light is coupled into the waveguide. The remaining light diffracts and gets scattered at the waveguide's borders. When the probe beam propagates coaxially with the waveguide, only the TEM_{00} transverse mode will be excited, which is illustrated in Fig. 18(a). Note the elliptical shape of the guided beam and the dark (defocusing) domains at either side, where the refractive index change is negative according to the anisotropic model depicted in Figs. 3 and 4. Higher-order modes of the waveguide can be excited by shifting the probe beam a few micrometers with respect to the center of the waveguide. Then, only a part of the intensity of the probe beam will be coupled into the waveguide, thereby selecting a certain range of transverse k-vectors. As a result, the light intensity confined by the waveguide propagates non-paraxially as a higher-order mode. This method as well as the excitation of modes by slightly tilting the probe beam are generic for all kinds of linear waveguides [79]. In the configuration of Fig. 18(b) the vertical shifting of the probe beam of $15\ \mu$m led to the excitation of a TEM_{01} mode. Shifting the probe beam for another $15\ \mu$m excited the TEM_{02} mode as shown in Fig. 18(c). In contrast, it is not possible to excite any TEM_{10} or TEM_{20} modes. The inherent anisotropy of the waveguide is reflected in its modal structure, since higher-order modes can predominately be excited in the vertical direction, perpendicular to the external electric field. According to numerical simulations [83] this behavior is based on a general rule that horizontal modes can only be excited when the transverse size of the waveguide exceeds the typical soliton diameter of $\approx 15\ \mu$m.

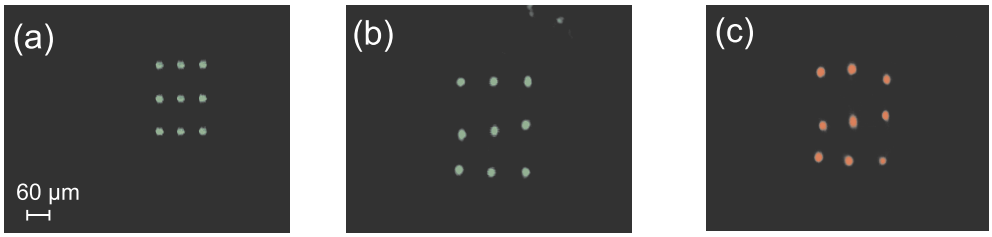

Fig. 19 Realization of a 3×3 waveguide array induced by photorefractive solitons. (a) Front face of the crystal where the spot-array is imaged (distance between spots $\delta x = 60$ µm,$\delta y = 80$ µ m; intensity in every channels 110 nW; diameter of each spot 15µm). (b) Array of 9 focused solitons, (c) waveguiding in separate channels of the array of a probe beam at $\lambda = 633$ nm

5.2 Arrays of photorefractive soliton waveguides

The parallel nature of optical information processing suggests the extension of soliton waveguides to two dimensions. However, up to now only a few publications studied the parallel propagation of several spatial solitons [86, 87]. To our knowledge, none of these were performed for the special case of a photorefractive nonlinearity so far. A crucial point in the parallel propagation of photorefractive spatial solitons is their anisotropic mutual interaction as described in chapter 4. Because the refractive index modulation induced by each single soliton reaches beyond its effective waveguide, phase-dependent coherent as well as separation-dependent incoherent interactions as repulsion, attraction or fusion may appear. These interaction effects also affect the waveguiding features in a soliton channel. Therefore, the parallel propagation of a multitude of solitons can only be achieved if the separation is carefully chosen in such a way to prevent all forms of interactions.

To create an array of solitons in a photorefractive crystal, the typical setup of soliton formation (see Fig. 6) was modified in such a way that the laser beam derived from a frequency-doubled Nd:YAG-laser emitting at $\lambda = 532$ nm illuminates a spatial light modulator, which imprints the image of a spot array onto the beam. Passing a set of different lenses the spatial light modulator is imaged onto the front face of a photorefractive SBN60:Ce crystal.

For the creation of a soliton array and its waveguiding properties, a regular pattern of 9 spots each with a diameter of 15 µm and an intensity of ≈ 110 nW is imaged onto the front face of the crystal (Fig. 19(a)). In the linear case – without applied electric field – the beams diffract on their way through the crystal and display a typical interference pattern. Applying the external electric field, self-focusing in this now nonlinear material forms an array of solitons without interaction (Fig. 19(b)). To obtain a propagation without mutual interaction, we take care that the initial distance between single channels is just large enough to prevent soliton interactions. Therefore, the horizontal and vertical initial separations are chosen to be $\Delta x = 60$ µm and $\Delta y = 80$ µm in order to exceed the coverage of the different transverse interaction effects.

A distance smaller than the critical distance for coherent interactions between the solitons in either case would cause the solitons to fuse uncontrollably due to their own mutual attractive force. The enlargement of the array compared to the spot array at the front face is due to the imaging optics, while the slight deviation of the symmetry is due to inhomogeneities of the crystal. To test for the waveguide properties of the single channels of such a soliton array, the wavelength selectivity is exploited to scan the soliton array with an intense red probe beam

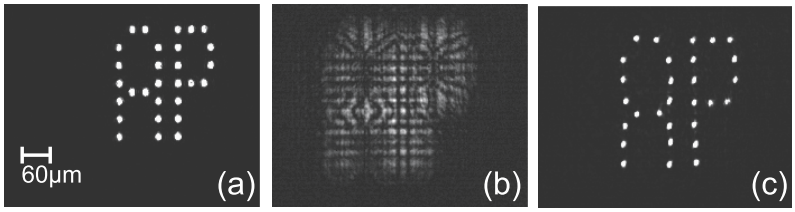

Fig. 20 Application of soliton waveguide arrays to focus depth enlargements in images. (a) front face of the crystal where the spot-array is imaged, (b) interference pattern due to linear propagation of the beams, (c) array of solitons

without significantly destroying the single soliton channels. Positioning the red probe beam successively to the positions of the previously induced solitons on the crystals front face, we find the probe beam to be guided in each of the nine channels solely. The scan of this array with the red probe beam is shown in Fig. 19(c). To obtain information of the complete array, every single channel is scanned separately, and the nine individual images are superimposed electronically.

Naturally, larger arrays of solitons can also be formed. Their number is mainly limited by the aperture of the photorefractive crystal and the resolution of the inducing spatial light modulator. In larger arrays, several applications of parallel soliton and waveguide formation can be imagined. As an example, digitized images consists of large arrays of pixel-like spots arranged on a square lattice. In the linear regime, such an image can be reconstructed only in a range that is limited by the depth of focus of the imaging optics due to the blurring effects of diffraction. However, if these arrays of spots are propagating in a nonlinear, solitonic regime, we are able to enlarge the range of focus depth to the length of the soliton formation, i.e. to the length of the nonlinear crystal. This idea, first suggested by [86], has also been demonstrated by our group with a regular pattern of 25 spots with a diameter of 15 μm and an intensity of ≈ 20 mW/cm^2.

The formation of larger soliton-patterns in principle is not limited to symmetric arrays. Consequently, and as an extension of this idea, reconstructions of selective array configurations that correspond to images, can be processed. Fig. 20(a) shows the configuration of the letters "AP" at the front face of the crystal, Fig. 20(b) illustrates the corresponding blurred image resulting from the linear diffraction when the external voltage is switched off and Fig. 20(c) depicts the reconstructed image when the voltage is applied.

5.3 Soliton-induced couplers and Y-junctions

In the previous sections we demonstrated that both separate effects of waveguiding and scalar interactions of spatial solitons may lead to fascinating and rather complicated light configurations. Combining these effects leads to the demonstration that waveguiding in interacting solitons can be exploited to design a whole variety of different waveguide couplers and dividers.

Here, we restrict ourselves to the demonstration of the capability of guidance of two incoherent interacting solitons. For this case, two different cases of soliton interaction can be distinguished. Depending on the initial launching conditions (mutual distance and direction), the two simultaneously propagating solitons can display attraction, separation, rotation or even

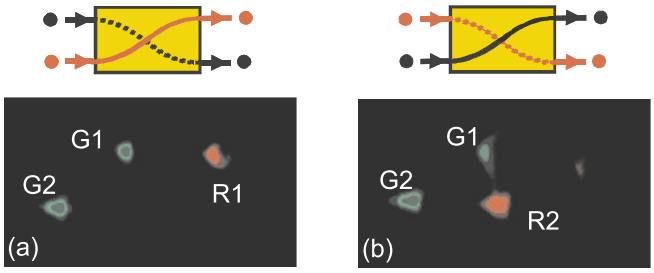

Fig. 21 Independent guidance of a beam in two interacting solitons in a configuration that induced a rotation of the solitons amongst each other. The figures show the guidance of the probe beam R in (a) the soliton G1 and (b) the soliton G2

a spiraling motion, accompanied by a mutual exchange of energy [72]. In interaction scenarios of parallely propagation solitons, where attraction, repulsion or rotation can be expected, a soliton which guides a signal wave can be moved to another position by launching a second soliton as a controlling beam. This function is the basis for every adaptive all-optical switch. In order to demonstrate such a scenario, two beams G1 and G2 each with an intensity of $I \approx 30$ mW/cm^2 are focused onto the crystal's front face. Their initial diameter is about $d_x \approx 15\ \mu\mathrm{m}$ in x- and $d_y \approx 5\ \mu\mathrm{m}$ in y-direction. When self-focusing of the beams starts, the two solitons form and interact strongly and their propagation plane rotates about an angle of $60°$. Coupling a He-Ne-laser probe beam R ($\lambda = 633$ nm) into either one of the soliton channels, the probe beam can be found to be guided only in this particular soliton without energy coupling into the other soliton. An example of such a situation is shown in Figs. 21(a),(b) where the probe beam is guided in the soliton G1 or G2 respectively. Similar to Fig. 17 the probe beam appears laterally shifted with respect to the writing beams G1 and G2 due to the wavelength selective prism in front of the camera. Even though the beams do not propagate in a perfect solitary form, the probe beam R is guided properly in the structure written by the beam G1 or G2 (Figs. 21(a),(b)). To use this situation as an all optical switch i.e. beam G2 can be used as a steering beam for the beam G1, guiding the signal beam R.

For an interaction scenario with a mutual exchange of energy, waveguiding is expected to result in a splitting of a single beam among several soliton channels. To investigate this feature, the two interacting beams are launched in a skewed way into the photorefractive crystal, thereby inducing an angular momentum comparable with the scenario of spiraling scalar solitons depicted in Fig. 16. For that purpose, the two writing beams G1 and G2 are launched with a lateral distance of approximately one spot diameter ($d_x \approx 15\ \mu$m) and at a relative angle of approximately $0.1°$ towards each other. The mutual exchange of energy of the two solitons can easily be proved in blocking one of the beams, which results in a light intensity which is still apparent in both channels at the back side of the crystal. Due to the persistence of the waveguides once written in our sample, the probe beam can be guided easily while the writing beams are blocked. Therefore, we illustrate the back face of the crystal for such a configuration in Fig. 22(a). When directing the probe beam R to one of the soliton channels at the front face of the crystal, one finds the intensity of the probe beam to be guided in both channels. This situation is shown in Fig. 22(b) and (c) where we couple the probe beam into the soliton channel G1 or G2, respectively. In both cases the principle division of the probe beam is obvious. Due to the complex interaction of the beams on their way through bulk material, the solitons loose their identity for the benefit of a multi-soliton complex, which leads to crosstalk of the waveguiding structure. Therefore, by exploiting the features of energy-exchanging soliton interaction, an effective y-coupler can be created.

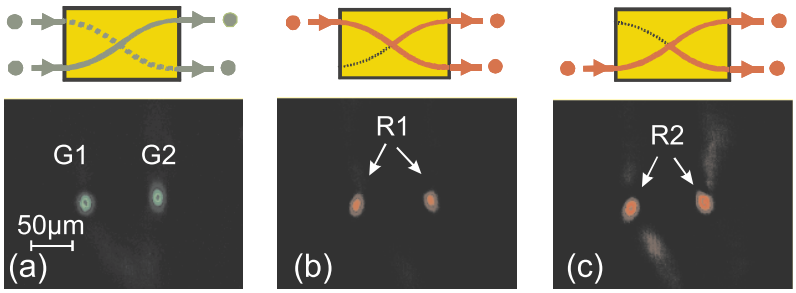

Fig. 22 Division of a probe beam R due to the incoherent interaction of two solitons G1, G2. Crystal's exit face when the solitons G1 and G2 fulfill a spiraling motion inside the bulk material (a). The red probe beam R splits into two channels when it is coupled into the soliton channel G1 (b) or G2 (c)

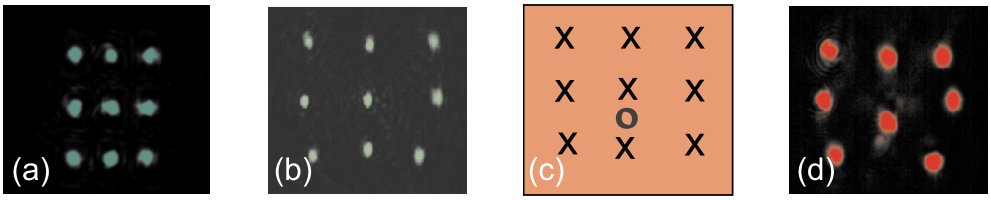

Fig. 23 Optical control of a soliton array. (a) The spot array at the entrance face of the nonlinear crystal (distance between spots $\delta x = 50$ µm, $\delta y = 70$ µm; diameter of each spot of 12µm), (b) the uncontrolled soliton array, (c) sketch of the position of the steering soliton beam, (d) the controlled array probed by a beam at $\lambda = 633$ nm

5.4 Interaction in waveguide arrays

With the experimental realizations in the previous sections – the formation of soliton arrays and soliton interactions for waveguiding purposes – we have all tools available to realize steerable interconnections of waveguide arrays. In order to demonstrate an example of the various interaction scenarios we demonstrate a controlled interaction between two distinct channels of a 3x3 soliton array. To manipulate the mutual attractive interaction between coherent spatial solitons, a third beam positioned between two adjoining channels, is used to steer the distinct spots of the soliton array. Therefore, a separate beam derived from the Nd:YAG-laser is focused appropriately onto the front face of the crystal. While in this experiment each soliton of the array has an intensity of $I \approx 55$ mW/cm^2, the additional steering beam is about three times stronger. In Fig. 23(a), the front face of the crystal with the uncontrolled array is shown, with a lateral distance between the single spots of $\Delta x = 50$µm, $\delta y = 70$µm and a spot diameter of 12µm (FWHM). Fig. 23(b) displays the undisturbed array of solitons after a propagation of 20 mm in the biased crystal. Once the control beam is positioned between the central lower two solitons, which is depicted by the sketch in Fig. 23(c), the new soliton array forms which leads to the attraction and subsequent fusion of the central and the lower central spot. Fig. 23(d) shows the probe beam of $\lambda = 633$ nm guided in each channel of the controlled array separately (again the single snapshots are superimposed electronically). Nevertheless, the fusion of the two lower

middle channels is obvious, creating a y-coupler within the waveguide array. Therefore, the case of coupling the probe beam into the central or the lower middle channel on the front face of the crystal reveals an effective guiding into the same output, respectively.

In principle, the fusion of neighboring channels in the direction of the electric field is also possible. In this case however, the distance between the control beam and each channel has to be smaller than in the y-direction in order to compensate for the different coherent interaction coverage.

These examples show clearly that all-optical control of single channels of soliton arrays is possible by inducing a determined interaction within the waveguide array. Although these first experiments focus on coherent interactions, the case of mutually incoherent beams is even more promising, allowing to realize rotations and energy exchanges between definite spots of large arrays. With these tools it is possible to realize all-optical, adaptive processing elements that include all scenarios necessary for complex optical interconnection tasks.

6 Vector solitons

Vector solitons consist of different components of comparable intensity and contribute equally to the induced refractive index modulation of the material. The participating optical beams induce a joint refractive index modulation in which they propagate self-consistently as eigenmodes. This it totally different to the waveguiding approach describe in chapter 5, where only one beam creates an effective refractive index waveguide in which another beam, typically of different wavelength is only guided passively. The essential requirement for vector solitons is the absence of any interference between the single components, which can either be achieved by using beams of different wavelength, different polarization [36] or just mutually incoherent beams. Because photorefractive materials are highly wavelength sensitive and the refractive index change due to the electro-optic effect depends on the plane of polarization, the only effective approach to destroy the mutual coherence between the single components without changing the electrooptic properties is to make the beams incoherent with respect to each other. Experimentally, this can be realized with the same technique as described above for incoherent interactions of scalar solitons (i.e. Section 4.2 and Fig. 8). The single beams of the vector solitons are typically of different geometry which can be realized by imprinting a required phase- or amplitude modulation on one of the two beams.

For the (1+1)D geometry, incoherently coupled soliton pairs have been predicted to exist in photorefractive nonlinear materials in 1996 by Christodoulides et al. [88] and subsequently demonstrated experimentally by Chen et al. [89]. It could be demonstrated that a modulation instability that appeared for each separate beam could be suppressed when both beams propagate simultaneously. Each beam itself does not propagate in a stable way, because the external parameters are not within the soliton existence range. When both beams propagate simultaneously, the total intensity increases and the parameters shift towards a domain of stable solitons. Pairs of bright – as well as bright-dark pairs – of photorefractive solitons were realized [89].

In 1998 the first observation of composite multimode solitons in photorefractive medium has been reported by Mitchell et al. [90] who demonstrated the stable propagation of (1+1) dimensional higher-order mode solitary beams. It these experiments the typical transverse spreading of multi-humped optical beams could be prevented in the presence of a fundamental stripe beam of Gaussian shape. Multi-humped beams, that represent higher-order transverse

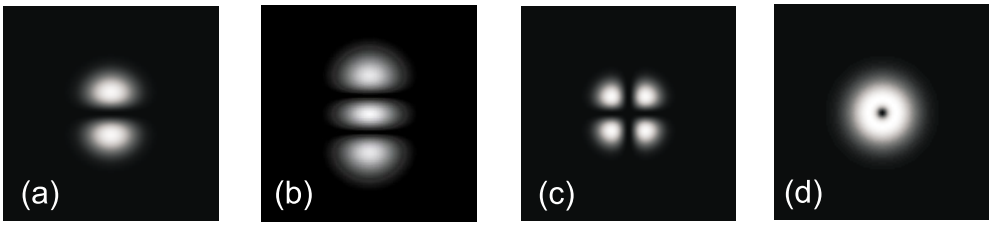

Fig. 24 Illustration of some low-order transverse modes. Intensity pattern of a Hermite-Gaussian HG_{01}(a), HG_{02}(b), HG_{11}(c) and Laguerre-Gaussian LG_{01} (d) modes

modes of a waveguide, typically display one or several π–phase jumps across their transverse plane which leads to a mutual repulsion of the single beamlets when they propagate in a self-focusing medium. In principle this behavior is directly comparable to the coherent interaction described in Section 4.1. The authors of [90] demonstrated various stable combinations of such multi-humped multi-component light structures consisting of a fundamental and a double-humped or even triple-humped mode. Their stability was subsequently analyzed by a linear stability analysis [91, 92], which revealed that only the fundamental double-humped pair is modulationally stable, whereas all higher-order modes of triple-humped type become subject to instability for larger propagation distances, which could not be revealed experimentally due to the limited length of the crystal sample.

As for the case of scalar beams, the expansion from a one-dimensional to a two-dimensional transverse system of vector solitons is a non-trivial task. In contrast to the one-dimensional system the realization of multi-humped beams in two dimensions promises a manifold of possible configurations because of the additional transverse dimension. Therefore, higher-order mode beams can display either a transverse or circular symmetry, similar to transverse laser modes of Hermite-Gaussian or Laguerre-Gaussian type, respectively. (2+1)-dimensional vector solitons of radial symmetry bearing a topological charge have been predicted for an isotropic threshold nonlinear model [93, 94], but shown to be modulationally unstable in a medium with a saturable nonlinearity [95]. This numerically found instability shows a distinct breakup behavior that leads to the generation of a *dipole-mode vector soliton* that has been subject to numerous investigations [95–100].

6.1 Vector solitons of Hermite-Gaussian and Laguerre-Gaussian type

In Fig. 24, we illustrate several transverse modes of Hermite-Gaussian and Laguerre-Gaussian type, that may serve as higher-order constituents of a two-dimensional vector soliton. Fig. 24(a) depicts a dipole-like Hermite-Gaussian mode (HG_{01}), that consists of two bright lobes separated by a dark vertical notch with a π-phase jump across its vertical direction. Introducing two phase jumps of π either leads to a triple-humped HG_{02} or to a quadrupole-like HG_{11} mode, illustrated in Fig. 24(b) and (c). Whereas all modes of Hermite-Gaussian type display a vertical and horizontal symmetry axis, the doughnut modes of Laguerre-Gaussian type in Fig. 24(d) are radially symmetric. The transverse phase distribution of a doughnut mode varies azimuthally and covers $\Delta\phi = 2\pi m$ for 360°. Moreover, a phase singularity exists in the central region of the mode, where the intensity drops to zero. The integer m indicates the mode's topological charge. In experimental realizations, a vortex beam reveals clearly by interference with a

plane- or spherical wave [101]. In case of the plane-wave-interference, the phase singularity manifests via the splitting of one single interference stripe into $m + 1$ stripes. In contrast, interference with a spherical wave shows a helical structure from which the commonly used name *optical vortex* was derived. Investigations on the stability of optical vortices while propagating through a nonlinear self-focusing medium revealed hat they do not propagate self-consistently [27, 64, 101]. Moreover, multiply-charged optical vortex beams disintegrate via a two-step mechanism [102]. A vortex with $m = n$ $(n > 1)$ first decays into n singly-charged optical vortices $(m = 1)$ which in turn become subject to further disintegration.

The experimental generation of the dipole beam depicted by Fig. 24(a) can be realized by partially inserting a thin glass slide into the beam. That part of the beam which is transmitted through the glass slide experiences a phase shift due to the different refractive index. A phase shift of π can be realized by varying the optical path length in the glass slide by tilting the slide with respect to the optical axis. Higher-order mode beams as depicted in Fig. 24(b),(c) can be realized by applying two glass slides in different transverse directions or by superimposing several mutually coherent beams with the required relative phase shift. The generation of an optical vortex is not as straightforward but can be realized with the help of computer-generated holographic phase masks. Transmission of an optical beam through the phase mask will then produce the required beam shape in the first and minus first diffraction order.

6.1.1 Lowest-order (2+1)-D vector solitons

Musslimani et al. [93] demonstrated numerically that two-dimensional vector solitons carrying a topological charge do exist in a self-focusing threshold nonlinear medium. The typical break-up of an optical vortex can be prevented in the presence of an additional co-propagating beam with a node-less shape, e.g. a Gaussian beam. In this way, a light beam with a complex internal geometry that does not propagate self-consistently itself in self-focusing media can be stabilized when combined with a mutually incoherent fundamental beam. After this prediction of multi-component solitary beams in both transverse dimensions, Garcia et al. [95] revealed that these solitary solutions of a Gauss-vortex-pair is modulationally unstable and disintegrates into a azimuthally rotating dipole structure after a fairly long propagation distance. The structure has been reported to maintain its shape for some 10 diffraction lengths before the inherent numerical noise leads to the described instability. This instability is demonstrated in Fig. 25 in an isosurface plot for $I = 0.15 I_0$ and $z = 100\ L_d$. The simulation depicted in Fig. 25 is based on the isotropic model and shows that the propagation of the vortex component is first accompanied by some minor oscillations of the beam diameter but finally disintegrates into two spiraling lobes that resemble a rotating dipole structure. As the propagation distance increases it becomes also apparent that the rotation period decreases due to continuous radiation losses, which can be interpreted as *friction* in terms of the particle model for solitons.

Our further investigations are twofold. First, it is interesting to know if such a breakup that occurs in an isotropic medium can be observed in an anisotropic experimental system. Second, does the evolving dipole-like light structure represent a mode of a stable vector soliton?

To investigate these open questions experimentally, we slightly modify the experimental setup depicted in Fig. 8 in such a way that one of the two mutually incoherent beams is transmitted through a computer-generated holographic phase mask in order to obtain the desired vortex mode with $m = 1$. Both beams are then superimposed and focused into the crystal. Fig. 26(a) depicts the incident light intensity of the vortex component – and its rather filamented structure after propagating 10 mm in the crystal separately (Fig. 26), which has already been

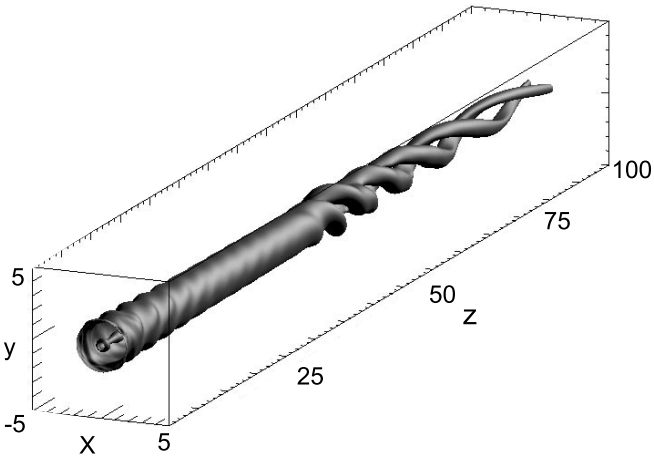

Fig. 25 Evolution of the vortex component of a vortex-Gaussian vector soliton on the basis of an isotropic simulation. The presence of the Gaussian beam prevents the transverse spreading of the vortex that decays after $z = 50L_d$ into an azimuthally rotating dipole mode

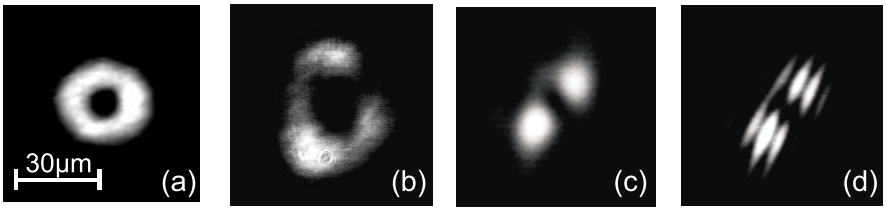

Fig. 26 Propagation of an optical vortex $(m = 1)$ in the photorefractive crystal. Incident vortex (a) and its break up after a separate propagation of 10 mm in the biased crystal (b). Simultaneous propagation with a mutually incoherent Gaussian beam leads to a tilted dipole structure (c)

observed in previous studies [64]. When we superimpose an incoherent Gaussian beam of equal total power, the vortex component transforms into a tilted double-humped structure which is depicted in Fig. 26(c). By visualizing the phase distribution via an interference with a plane reference wave (Fig. 26(d)), we are able prove that the two lobes are π out of phase. Thus we conclude that the vortex transformed into a dipole mode [96]. The general breakup behavior is in good agreement with the isotropic numerical simulations of Garcia et al. [95]. Albeit the decay into the dipole-structure can be observed in the isotropic simulation as well as in the inherently anisotropic experimental system, it occurs at a totally different stage of propagation. Whereas we observe the breakup after about 3.5 diffraction lengths in the experiment, it occurs roughly at a 10 times larger propagation distance in the isotropic simulation. This indicates that the role of anisotropy is of major importance for the propagation of circular symmetric light structures. As soon as the circular symmetric vortex beam propagates in the nonlinear medium it experiences the non-uniform refractive index modulation depicted in Fig. 3 that may lead to an immediate disintegration and hence leads to the decay into the dipole structure. Therefore, the more realistic anisotropic model has to be applied to reveal the propagation dynamics of the vortex component. In contrast to the isotropic simulations, the numerical beam propagation on the basis of the anisotropic model reveals a typical decay at about one diffraction length which corresponds to the experimentally observed situation. In a recent publication, Belić et

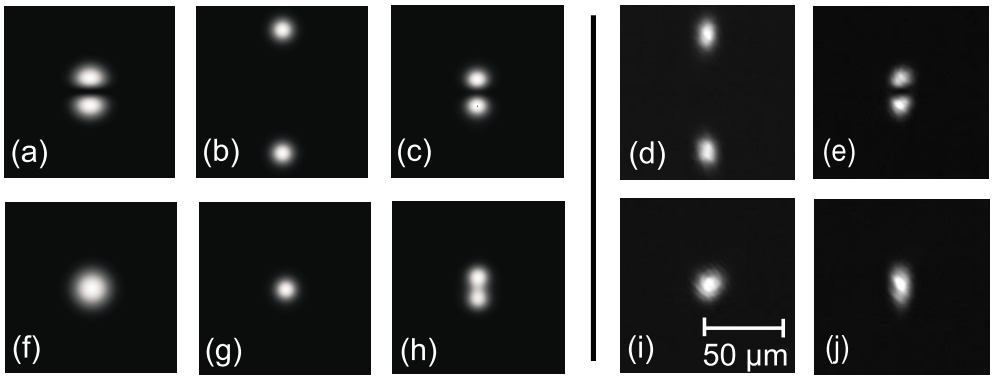

Fig. 27 Numerical (left) and experimental (right) generation of a dipole-mode vector soliton. The dipole and fundamental components are depicted in the upper and bottom row, respectively. Incident light intensity in (a),(f) and the diverging beamlets for a separate propagation of $z = 6.95\ L_d$(b), or $z = 20\ \mathrm{mm}$(d). Simultaneous propagation leads to a self-confined light structure (c),(h) and (e),(j). The repulsion of the dipole lobes (a),(e) is prevented in the presence of the Gaussian beam

al. [103] demonstrate the difference of the two models and reveal that the anisotropic model does not support a homogeneously rotating but a rather twisting and oscillating motion of the resulting dipole component. In analogy to the case of interacting incoherent solitons, the two dipole lobes preferably align along the vertical y-axis perpendicular to the externally applied electric field which is a stable orientation in a biased photorefractive crystal [100].

In order to verify whether the evolving dipole structure really represents a component of a stable vector soliton, we generate a dipole beam with the above-mentioned method directly which is then superimposed with a mutually incoherent Gaussian beam of equal total power. Figs. 27(a),(f) depict the initial intensity distributions of the dipole and Gaussian beam of equal total power in a numerical simulation (left) and in an experiment (right). In principle, the dipole beam can be thought of as two out-of-phase beamlets that become self-trapped in the nonlinear medium and display the soliton-typical repulsive coherent interaction (Figs. 27(b),(d)). The Gaussian component in contrast forms an ordinary photorefractive soliton as it propagates separately in the crystal (Figs. 27(g),(i)). The situation changes dramatically when both beams are co-propagating simultaneously, see Figs. 27(c),(h) and (e),(j). The formerly natural separation of the dipole lobes is prevented (Figs. 27(c),(e)), whereas the Gaussian component becomes elongated in the direction of the dipole-axis and adapts slightly a double-humped shape(Figs. 27(h),(j)). This observation demonstrates a generic feature of unstable structures that co-propagate incoherently with a stable soliton beam: both beams are now constituents of a stable and very robust soliton, a so-called *dipole-mode vector soliton*. These experimental results (right side of Fig. 27) are in excellent agreement already with the predictions of the isotropic simulations depicted in the left side of Fig. 27 and constitute the first experimental observation of this novel type of multi-component soliton, a dipole-mode vector soliton. It has been reported independently by two groups [96, 97].

We like to emphasize, that this phenomenon can not be understood in terms of a linear waveguide theory, since both beams contribute equally to the nonlinear index change. The Gaussian component of the dipole-mode vector soliton does not only serve as a stabilizing

component but it is also affected by the dipole mode. As a consequence, it becomes elongated in the direction of the dipole mode.

The aspect of the dipole-mode vector soliton's stability and transverse shape is extensively investigated in [98] where we make use of a two-beam expansion of the Petviashvili approach (compare Section 3.4.1). In this work we explore the parameter space for numerically exact soliton solutions of the anisotropic photorefractive model. For a given external voltage the relative beam power $P_{\mathrm{Gauss}}/P_{\mathrm{Dipole}}$ can range from almost infinity to 0.3, which in turn leads to a Gaussian- or dipole-dominated shape of the resulting vector soliton. In the limit of a vanishing dipole beam, the entire complex can be considered as a scalar soliton that is derived from a Gaussian beam.

In the other limit, the separation of two dipole lobes increases as the power of the Gaussian beam decreases, which in turn becomes more and more elongated in the vertical direction and even adapts the dipole structure. We were even able to demonstrate this specific characteristics experimentally that displays an excellent agreement with the numerical parameters. In the limit of a vanishing fundamental mode, the specific property of the photorefractive response leads to the formation of a bound dipole soliton, that has been investigated by Mamaev et al. [104].

Another direct consequence of the anisotropic nature of the photorefractive nonlinearity reveals in the fact that the dipole-mode vector soliton preferably aligns along the vertical direction, perpendicular to the applied electric field [100]. In terms of a particle model, this represents a state of lowest potential energy for the vector soliton, and therefore can be considered as a global minimum. If the dipole-mode is launched at a non-zero azimuthal angle with respect to the vertical axis, it starts to oscillate around its stable vertical orientation. Additionally, there exists a local minimum when the dipole is oriented in the horizontal direction parallel to the external field. This state is not modulationally stable since the double-humped structure will align in the vertical direction again, when it is slightly disturbed. In this way the anisotropic nature of the refractive index modulation not only reveals via the distinct shape and interaction of scalar solitons but as well and especially in the formation and stability of vector solitons.

From the above discussion it is obvious e.g. in the spiraling of interacting scalar solitons and the decay of a vortex-mode that the photorefractive nonlinearity does not directly support the continuous rotation of light structures in the transverse plane, but tends to transform any kind of angular momentum into a twisting or oscillating motion.

6.1.2 Higher-order mode vector solitons

The robustness of the dipole mode vector soliton motivates an extension of the investigations to higher-order multi-humped solitary waves. Since multi-humped multi-component (1+1)D light waves become subject of modulation instability for the local and isotropic model [91], we investigate the generation of higher-order mode and multi-pole vector solitons on the basis of the anisotropic nonlocal model. Thereby we want to reveal if these higher-order mode beams display a universal propagation characteristics.

In analogy to the breakup of a singly-charged vortex (see Fig. 26), we now investigate the propagation dynamics of a higher-order optical vortex in form of a doubly-charged $(m = 2)$ doughnut beam in combination with a fundamental Gaussian mode, expecting similar characteristics as the unstable propagation of singly– or doubly–charged optical vortices themselves [27,64]. In Fig. 28, we combine a doughnut beam of $1.7\,\mu\mathrm{W}$ with a mutually incoherent fundamental mode of comparable total power of $1.9\,\mu\mathrm{W}$ and proceed in the same way already

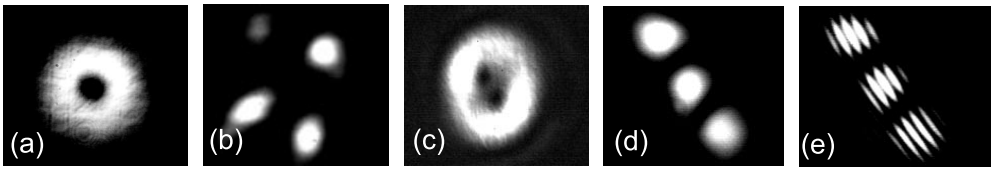

Fig. 28 Experimentally observed breakup (b) of an optical vortex $(m = 2)$ (a) and its successive decay into a twisting triple-humped structure (d) via an intermediate state two singly charged vortices (c) in the presence of a Gaussian beam

described above. Fig. 28(a) depicts the incident doughnut mode that displays a fairly disordered disintegration after 13.5 mm of separate propagation in the self-focusing medium in Fig. 28(b). In the presence of the Gaussian beam we flip the crystal in order to investigate a propagation of 5 mm along the crystallographic b-axis and observe the light structure depicted by Fig. 28(c). A distinct deformation of the initially circular symmetric beam and the evolution of two dark notches in its center is clearly visible. With the help of an interference experiment we were able to connect each of the dark spots to a singly charged vortex [105]. Investigating the same beam configuration along the propagation distance of 13.5 mm and keeping the external voltage of 1.8 kV constant, we detect the decay of the vortex into a tilted triple-humped light structure which is illustrated in Fig. 28(d). In [105] we also compared these experimentally obtained results with anisotropic numerical beam propagation studies and reveal a good agreement.

According to our experiments, the Gaussian beam has a stabilizing influence on the propagation dynamics of topologically charged doughnut modes, which in turn is not strong enough to compensate for the decay into a well-defined multi-humped light structure. This is a strong confirmation of the universal effect that all topologically charged light beams transform into a rotating or twisting multi-humped object in self-focusing media [27, 64]. Additionally, we observe the well-known phenomenon [102] that an optical mode of charge m transforms into a $m + 1$ multi-humped light structure. Each initial phase singularity leads to a π-phase jump in the transverse profile of the mode in accordance to previous investigations. Comparing our numerical results in [105] with the propagation dynamics in an isotropic atomic vapor system [27] we conclude, that an oscillating transverse motion around the vertical axis stems from the inherent anisotropy of our photorefractive system. Finally, the additional Gaussian beam prevents a further separation of the single humps with increasing propagation distance. This is underlined by studies of the self-focusing properties of a triple-humped mode with a Gaussian beam that demonstrate the generation of a stable triple-humped multi-component soliton in a nonlocal anisotropic medium [105]. Similar to the dipole-mode vector soliton (refer 6.1.1), this specific triple-humped light structure tends to align in the vertical direction perpendicular to the externally applied electric field due to the anisotropy of the photorefractive medium.

Soon after the prediction of the dipole-mode vector soliton and its subsequent experimental observation [96, 97], numerous experimental and numerical investigations deal with the problem of stabilization of various multi-pole structures due to the co-propagation with a fundamental mode [99, 106, 107]. Desyatnikov et al. [107] demonstrate the existence of various types of composite solitary structures in the isotropic regime. A HG_{11}-mode with a π-phase jump across both transverse directions resembling a quadrupole structure as well as a hexapole and a dodecagon multipole can indeed serve as a higher-order component of a non-diverging

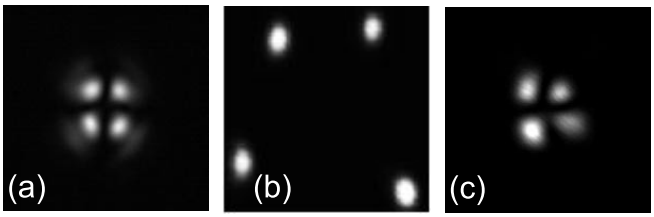

Fig. 29 Experimental observation of a quadrupole-mode vector soliton generation. (a) Incident HG_{11} -mode beam, and its diverging/non-diverging profile after a separate/coupled propagation of $13.5\ mm$ (b)/(c)

light structure and form a stable vector soliton in combination with a fundamental mode. In Fig. 29 we illustrate the formation of a quadrupole-mode vector soliton in an experiment. Fig. 29(a) displays the incident light intensity at the front face of the crystal and its diverging profile at the exit face of the biased crystal in Fig. 29(b). Each of the single beamlets forms a quasi-soliton that repel mutually due to their relative π-phase shift across the horizontal and vertical direction. When we superimpose a slightly stronger Gaussian beam of $2.7\ \mu W$, the repulsion of the four quadrupole lobes is completely compensated and the two components co-propagate self-consistently in the material which is depicted in Fig. 29(c). Again the isotropic simulation in [107] is in a good agreement with the experimentally obtained data, but when we rotate the quadrupole structure by 45° the anisotropy of the experimental system becomes apparent and the quadrupole structure undergoes a shape transformation that can only be simulated with the anisotropic model [106]. A single successful generation of experimental hexapole vector soliton has been reported [106], but the inherent anisotropy of the photorefractive nonlinearity merely leads to a disintegration rather than to a stable self-focused light structure. Highly symmetric transverse optical structures are quite difficult to realize due to crystal inhomogeneities and the inherent anisotropy if the photorefractive system. Other even more complicated geometries like double-ring flower modes [106] have not been demonstrated so far, and may even not be realizable.

6.2 Vector solitons due to mutual stabilization

Up to now, we achieved non-diverging structures due to the stabilizing impact of a fundamental mode. The question, if two or more unstable, diverging light structures can also mutually stabilize is therefore a crucial point for the general understanding of vector-solitons. This mutual trapping of a double- and a triple-humped mode has been first successfully demonstrated in a one-dimensional photorefractive system [90] but up to now never been observed in the two-dimensional configuration. From the scenarios described above it is obvious that neither the double- nor the triple–humped optical beam itself propagate self-consistently in a self-focusing medium. To investigate the propagation behavior of such a specific beam constellation, we create two mutually incoherent optical fields, depicted by Fig. 30(a),(d). When the two higher-order modes propagate separately for 13.5 mm in the nonlinear crystal, all their single beamlets form quasi-solitons. But due to their relative π-phase shift, they repel strongly as they propagate, which results in an increasing vertical separation as can be seen from Figs. 30(b) and (e), respectively. The simultaneous propagation in contrast, which is depicted in Figs. 30(c) and (f) leads to a mutual attraction of the single lobes and the overall spreading of the multi-component solitary wave minimizes. Comparing the incident light structures with those that evolve from the interaction in Figs. 30(c),(f) it is obvious that the shape of both higher-order modes becomes strongly affected. Especially the two lobes of the dipole as well as the innermost lobe

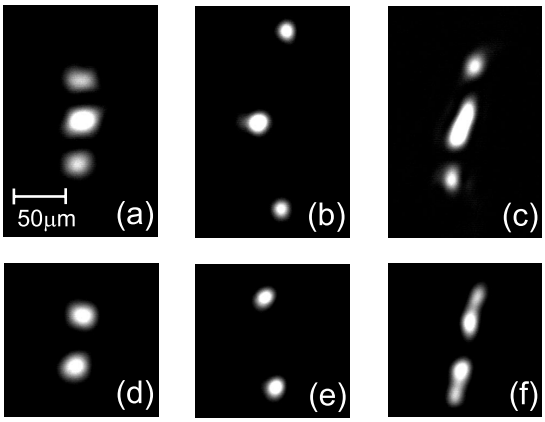

Fig. 30 Experimental observation of the mutual stabilization of a double– and a triple–humped mode. Incident light intensity in (a),(d), and the spatial spreading after $13.5\ \mathrm{mm}$ due to various π-phase jumps across the beams (b),(e), and the mutual attraction in the case of simultaneous propagation (c),(f)

of the triple-humped beam become strongly elongated in the vertical direction, which is a consequence of the mutual attraction of these neighbouring beamlets. Since the resulting light pattern deviates clearly from the initial conditions as depicted in Figs. 30(a),(d), and due to the limited propagation distance that is experimentally available, we cannot prove that these light structures do not eventually breakup when they propagate further. To gain more insight into the stabilization or an eventual breakup process we apply simulations of the anisotropic and non-local type that display comparable results [105]. The single beamlets also become strongly elongated and after propagation distances that exceed the experimentally accessible range the entire structure disintegrates and predominately forms a dipole-mode vector soliton. To reveal whether solitary solutions exist we apply the Petviashvili-based numerical procedure for this type of beam configuration. Our collaborating scientists were finally able to derive a soliton solution that displays stable and hence non-diverging propagation characteristics [108]. These numerical solutions reveal that especially the transverse shape of the single beamlets plays a major role for the stability of these multi-component structures. The continuous realization of various different beam shapes, that would be necessary to perform further experimental studies is an almost inaccessible control parameter. Taking into account that we launch beams with a Gaussian shape into the crystal that deviate clearly from the numerically derived profile we are yet able to demonstrate a distinct effect in Fig. 30. Generally speaking, we are able to demonstrate the striking effect of the mutual stabilization of inherently diverging higher-order mode optical beams.

6.3 Controlled breakup of multi-component light structures

Recently, Desyatnikov and Kivshar [109] demonstrated the formation and propagation dynamics of a new type of solitary structure, a so-called *necklace-ring vector solitons*. Necklace beams have been suggested in non-saturable Kerr-media [87] as beams that display an azimuthally modulated, ring-like intensity profile with π-phase shifts between adjacent lobes. They show remarkable propagation dynamics since they do not disintegrate in a bulk Kerr-medium but propagate in a stable way for fairly large propagation distances of up to 50 diffraction lengths. Due to the inherent phase configuration of the necklace, the structure sooner or later spreads in the transverse dimension depending on initial conditions. One approach to compensate

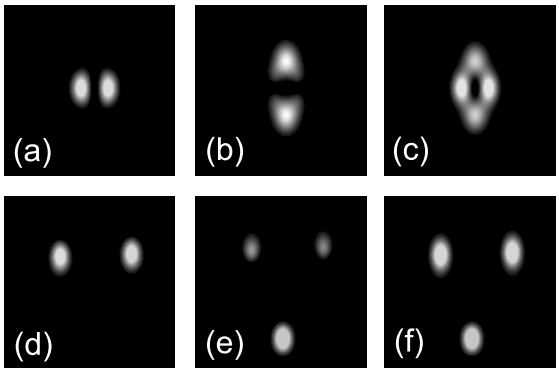

Fig. 31 Numerically obtained solution of two perpendicularly oriented dipole beams (a)–(c). Symmetry breaking instability after a numerical propagation of $\xi = 16$ is depicted in (d)–(f). Evolution of the horizontal and vertical dipole mode is shown in the first (a),(d) and second (b),(e) column. Total intensity is given by (c) and (f), respectively

for the spatial spreading of these necklace beams consists of applying the principle of vector solitons via the coupling of mutually incoherent necklace beams whose single lobes attract each other [109].

The simplest ring-like structure that represents such a necklace beam consists of two perpendicularly-aligned mutually incoherent dipole modes. In [109] it has been demonstrated that two perpendicularly oriented dipole-modes can indeed form a multi-component solitary ring-structure in an isotropic saturable self-focusing material. The repulsion of two oppositely located dipole lobes can be compensated by the mutual attraction of adjacent lobes that are mutually incoherent. A stability analysis via numerical beam propagation reveals an astonishing symmetry-breaking instability. The ring-like structure splits into three single lobes, positioned at the edges of a regular triangle, that separate radially with increasing propagation distance.

In order to account for the experimental conditions of a circular symmetric incident light structure, we applied the Petviashvili-method (see e.g. 3.4.1) to simulate the anisotropic experimental system as realistic as possible [110]. Hereby, we obtain a horizontally squeezed ring-like solitary solution which in turn shows a similar triangular-like symmetry-breaking instability when it becomes subject to perturbations. The principle characteristics of this dipole-dipole coupled pair is displayed in Fig. 31. The profiles of the incident horizontal and vertical dipole components depicted in Figs. 31(a),(b) result from the Petviashvili-based simulation. The separation and the shape of the horizontal dipole lobes in Fig. 31 vary slightly from those of the vertical component in Fig. 31(b) due to the inherent anisotropy of the medium. As a result, the overall intensity depicted in Fig. 31(c) resembles rather a horizontally squeezed ring than a circular symmetric structure. Nevertheless, when both components co-propagate mutually incoherent in the self-focusing material the repulsion of the oppositely located lobes, that are π-out of phase, is prevented and the entire structure remains unaltered. Due to numerical noise that stems from a quite rough discretization of the numerical array, the self-focused light structure starts to disintegrate at $\xi = 10$. The breakup characteristics displays a symmetry-breaking instability, since the two components split unequally in Figs. 31(d),(e) after $\xi = 16$, and the initial symmetry of the system is broken which reveals in the evolving triangular structure of the total intensity distribution in Fig. 31(f). Because the experimental implementation of the shape of the single lobes that are required to obtain the stable vector soliton-solution is beyond our technical capabilities, we approach the configuration of two coupled dipole modes with four Gaussian beams that are pairwise out of phase. The top row of Fig. 32(a)–(c) depicts various experimentally observed stages of propagation. The initial total intensity distribution

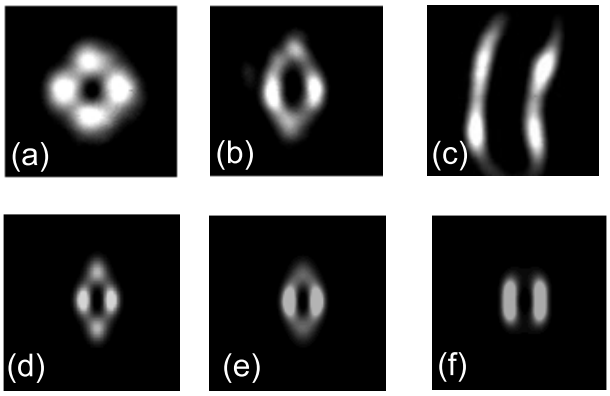

Fig. 32 Experimental (top row) and numerical (bottom row) implementation of the dipole-dipole coupled soliton pair. Total intensity at $z = 0$ mm (a),(d), $z = 5$ mm (b),(e) and $z = 13.5$ mm (c),(f)

depicted in Fig. 32(a) consists of the two perpendicularly oriented dipole modes, that do not exactly represent the desired shape from the numerical simulation depicted in Fig. 31(a)–(c). As the two dipole modes propagate in the material for 5 mm, we observe in Fig. 32 that both modes become strongly affected. The two horizontally-aligned lobes become clearly focused, whereas the vertically aligned ones become somehow kidney-shaped and torn in the horizontal direction. When we repeatedly flip the crystal sample and investigate the propagation along the 13.5 mm long a-axis for the same parameters of 2.3 μW of beam power for each mode, and an external voltage of 3.6 kV/cm, we detect a distinct breakup of the structure into two intensity-modulated stripes, which is depicted by Fig. 32(c).

The experimentally-observed scenario deviates from the numerical simulation depicted in Fig. 31. To account for these deviations, which we estimate to be due to different intensities in the components of the vertical and horizontal dipoles, we simulate the experimental propagation behavior by inducing a supplementary initial perturbation by changing the intensity of one component relative to the other by 10%. The additionally induced noise leads in fact to a different propagation behavior, which is depicted by the bottom row of Fig. 32. The initially perturbed soliton solution is illustrated in Fig. 32 and the spatial evolution after $\xi = 2.5$ and $\xi = 4.5$ which roughly corresponds to 5 mm and 13.5 mm of propagation distance is depicted in Figs. 32(e) and (f) respectively.

These results demonstrate an excellent agreement between the numerical and experimental breakup characteristics. According to the numerical evolution for larger propagation distances, the two arising stripes spread further in the horizontal direction, but remain self-confined vertically. This can be interpreted in terms of two dipole-mode vector solitons that separate in the horizontal plane.
The simulations as well as the experimental results demonstrate the mutual stabilization of two perpendicularly-coupled dipole-mode beams in an anisotropic self-focusing medium. Both optical modes propagate in a stable and non-diverging way for a few diffraction lengths before they become subject to a noise-induced symmetry-breaking instability. This distinct unstable propagation behavior in turn leads to a conversion of the vertical dipole mode into a horizontally spreading quadrupole-like structure. Therefore, the whole process can be interpreted as the controlled transformation of two dipole mode beams into two dipole-mode vector solitons.

6.4 Clusters of vector solitons

As illustrated above, the coupling of two perpendicularly oriented dipole modes leads to the formation of a semi-stable solitary light structure. By virtue of the well investigated effect that a fundamental Gaussian beam can trap or stabilize complex transverse light structures in order to become a higher-order component of a stable vector soliton, we now investigate the stabilization of the above-mentioned coupled dipole structure with the help of an additional Gaussian beam. In a recent numerical work [111], we could show that a configuration consisting of a two perpendicularly oriented dipole modes and a Gaussian fundamental beam can indeed form a non-diverging entity for the case of an isotropic saturable nonlinearity. These *multi-component dipole-mode solitons* were shown to exist in a wide range of the parameter space. Since the two dipole modes themselves bear a symmetry breaking instability, the power of the stabilizing Gaussian relative to the two dipole components is of crucial importance for the dynamical characteristics of this three-component object. We found an instability threshold when the power of the vertical or horizontal dipole mode exceeds a certain value and the beams propagate for an appreciable distance. In this case, an unstable soliton breaks the symmetry along both symmetry axes of the initial light distribution. The products of this instability typically evolve into a fundamental soliton and a rotating dipole-mode vector soliton that has recently been introduced as a *propeller soliton* [112]. Near the instability threshold, an even more intriguing dynamics accompanied by weak oscillatory instabilities arises. The symmetry is broken only along one axis leading to the formation of a fundamental, a dipole and a triangularly aligned triple-humped structure. The latter evolves from the weaker dipole mode and displays a fascinating *swinging dynamics* as it propagates further. We expect that these vibrational degrees of freedom, which are likely associated with long-lived soliton internal modes, should manifest themselves in the rich dynamics of soliton collisions.

Since the generation of a stable three-component solitary structure has been clearly revealed for an isotropic simulation, we expect to observe a comparable behavior in an anisotropic or photorefractive medium. In order to compare our experiments with the stable solutions, the Petviashvili approach was again used to find numerical solutions for the anisotropic case of nonlinearity [113]. It indicates stable solitary structures for a vast parameter space of various relative beam powers. We found that the power of the two dipole modes must not exceed a certain threshold value in order to achieve a stable object, because otherwise the Gaussian component is not capable to trap the two instability-inducing dipole modes. In contrast to the isotropic system described above, rotating dipole- or swinging dynamical behavior near the instability threshold has not been observed. In Fig. 33 we illustrate the numerical and experimental generation of such a three-component light object.

Fig. 33(a) depicts the total light intensity distribution of the numerically calculated (top row) and experimentally evolved light structure (bottom row) after propagating 10 mm in the biased crystal. Comparing the single frames in the top and bottom row, a remarkable agreement concerning shapes of the single components is obvious. We can clearly demonstrate the experimental evolutions of the incident beams of Gaussian shape into specifically elongated light structures which show a remarkable similarity to the numerically calculated profiles.

When perturbing the system by varying the initial intensity distributions, the structure breaks as a whole and displays a symmetry-breaking behavior already known from [109]. Thereby, the total intensity distribution evolves into a triangular structure, which is unequally distributed among its constituents.

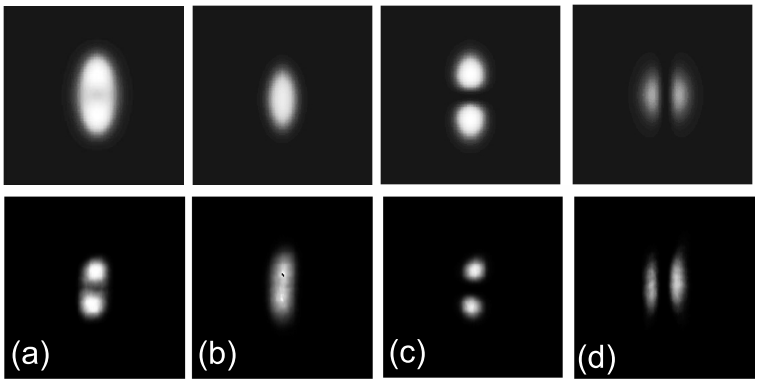

Fig. 33 Numerical (top row) and experimental (bottom row) formation of a multi-component vector soliton. Total intensity (a) and the contributions of Gaussian (b), vertical- (c) and horizontal dipole component (d)

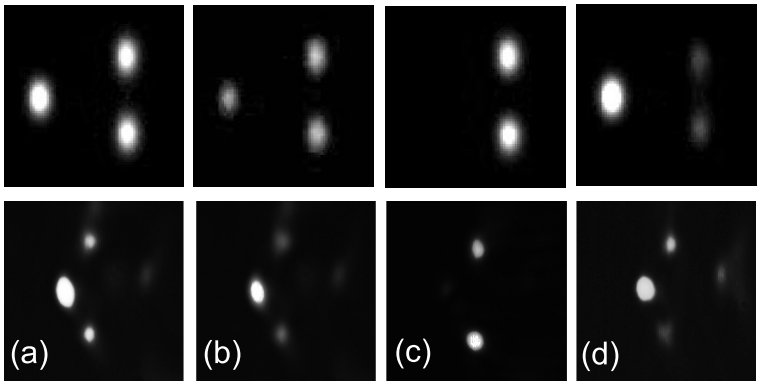

Fig. 34 Numerically (top row) and experimentally (bottom row) observed unstable propagation dynamics of a multi-component vector soliton. Total intensity (a) and the contributions of Gaussian (b), vertical (c) and horizontal dipole component

Fig. 34 illustrates this numerically and experimentally obtained instability in the top and bottom row, respectively. The total intensity distribution shows three spots of comparable intensity in Fig. 34(a). The Gaussian component distributes almost equally on the three spots (Fig. 34(b)), whereas the vertical dipole merely remains in its principle double-humped shape (Fig. 34(c). In contrast to the latter, the horizontal dipole mode reveals one well-distinct peak at its left side and two vertically aligned spots around its center. Again a striking similarity between numerical simulations and experimental results is obvious. It is clear that the anisotropic nature of the photorefractive nonlinearity leads to a symmetry-breaking instability of solitary structures when the external conditions do not satisfy for the exact solution.

In general, we have demonstrated that the principle of stabilizing optical beams of complex geometry leading to the formation of stable vector solitons is not restricted to a certain number of constituent mutually incoherent beams. We believe that even more complex solitary beam

configurations consisting of even more components such as rotating *soliton clusters* [114] can be realized.

Multi-mode spatial optical solitary beams bear another interesting feature since they also describe a light wave of partially spatial coherence [115]. The degree of coherence governs the diffraction of a light wave, and in general it is a non-trivial task to trap spatially incoherent light in a self-focusing medium [116]. On the other hand it offers the low-cost implementation of light sources such as light emitting diodes for the realization of all-optical switching devices. Recent investigations of spatially incoherent light in self-focusing media illustrate a whole variety of intriguing effects in nonlinear physics [117, 118], and even the self-focusing of white light from an incandescent light bulb has been demonstrated [119].

7 Summary

The photorefractive nonlinear system represents an excellent tool to investigate spatial optical soliton phenomena. Various generic effects that have been predicted theoretically, have become experimentally accessible due to the ease of implementation of soliton generation in these nonlinear crystals. We believe, that the characteristic phenomena presented in this article lead to a deeper understanding of nonlinear processes throughout nonlinear physical systems. After an introduction to general soliton characteristics, we focus on the experimental generation of solitons in a photorefractive crystal and their theoretical description. Thereby, we demonstrate that only an anisotropic model describes the formation and propagation dynamics of these solitary structures in a realistic way. We further demonstrate the impact of the two major charge carrier transport processes – drift and diffusion – on the generation of photorefractive screening solitons. Due to the drift of photo-excited electrons, a focusing refractive index structure forms in the material, whereas diffusion leads to an asymmetric refractive index structure that gives rise to a self-bending effect.

Solitons manifest in their interaction behavior, which is therefore investigated in chapter 4. In our specific photorefractive system we are able to demonstrate several generic soliton interaction effects such as fusion and fission of solitary beams as well as mutual repulsion and attraction and even the unique effect of *anomalous interaction*. Our aims are twofold since on the one hand, we demonstrated experimentally various effects known from general soliton theory and on the other hand, we principally designed miscellaneous all-optical information-processing devices based on photorefractive solitons.

In chapter 5 we demonstrate that due to the wavelength selectivity of the photorefractive response, solitons can even operate as an effective waveguide for light beams of a different wavelength. We implement an effective soliton-induced waveguide for a red laser beam that usually diffracts linearly in the nonlinear material. Further on, we show that this waveguiding is even of multi-mode nature since we are able to excite several higher-order modes. We also demonstrate, that waveguide dividers as well as all optical interconnects can be implemented with a photorefractive system and that the generic features of these effects can even be exploited for all-optical data processing.

Chapter 6 is dedicated to a rather new and very intriguing field of optical spatial solitons. Here, we demonstrate that the simultaneous co-propagation of several mutually incoherent optical beams can induce a joint refractive index modulation in the medium which therefore represents a multi-mode waveguide. In particular, we show the generation of various kinds

of multi-component or vector solitons, that consist of a multi-humped beam that usually decomposes in a self-focusing medium, but can spatially be confined via the interaction with a fundamental beam. We demonstrate, that especially circular symmetric doughnut beams undergo a symmetry breaking instability due to the inherent anisotropy of the photorefractive crystal. Further on, we reveal that such multi-component solitons can even be generated without a fundamental beam, which is demonstrated by the successful mutual stabilization of various higher-order mode beams.

This article conveys our recent work on the field of photorefractive screening solitons which has been processed in collaboration with several research groups. We like to thank Professor Kaiser and the Theoretical Nonlinear Dynamics group at TU Darmstadt and especially Kristian Motzek and Andreas Stepken for providing some of the numerical plots presented in this work. We are grateful to Professor Tschudi and his Light and Particle Optics group at TU Darmstadt for general support, and we appreciate the support by the German Academic Exchange Service (DAAD) for the funding of scientific exchange with the Australian National University (ANU), Canberra. Special thanks to Wieslaw Królikowski, Glen McCarthy, Barry Luther-Davies from the Laser Physics Centre at ANU as well as Yuri Kivshar and Elena Ostrovskaya from the Nonlinear Physics Group at ANU, for a fruitful and ongoing collaboration. We also appreciate enlightening discussions with Anton Desyatnikov, University of Münster. Finally, we acknowledge support from the Graduiertenkolleg "Nichtlineare Kontinuierliche Systeme" at the University of Münster, and the FAZIT foundation.

References

[1] G. A. Askaryan, Effect of gradient of high-power electromagnetic field on electrons and atoms, Zh. Eksp. Teor. Fiz. **42**, 1567 (1962) [Sov. Phys. JETP **15**, 1088 (1962)].
[2] M. Hercher, Laser-induced damage in transparent media, J. Opt. Soc. Am. **54**, 563 (1964).
[3] R. Y. Chiao, E. Garmire, and C. H. Townes, Self-trapping of optical beams, Phys. Rev. Lett. **13**, 479 (1964); see also: Phys. Rev. Lett. **14**, 1056 (1965).
[4] V. E. Zakharov and A. B. Shabat, Exact theory of two-dimensional self-focusing and one-dimensional self-modulation of waves in nonlinear media, Zh. Eksp. Theor. Fiz. **61**, 118 (1971) [Sov. Phys. JETP **34**, 62 (1972)].
[5] M. Segev, Optical spatial solitons, Opt. Quant. Electron. **30**, 503 (1998).
[6] N. N. Akhmediev and A. Ankiewicz, Solitons - Nonlinear Pulses and Beams (Chapman & Hall, 1997).
[7] N. G. Vakhitov and A. A. Kolokolov, Stationary solutions of the wave equation in a medium with nonlinearity saturation, Radiophys. Quantum Electron. **16**, 783 (1973).
[8] A. A. Kolokolov, Stability of stationary solutions of nonlinear wave equations, Izv. Vyssh. Uchebn. Zaved. Radiofiz. **17**, 132 (1974) [Radiophys. Quantum Electron. **17**, 1016 (1976)].
[9] E. W. Laedke, K. H. Spatschek, and L. J. Stenflo, Evolution theorem for a class of pertubed envelope soliton solutions,J. Math. Phys. **24**, 2764 (1987).
[10] J. J. Rasmussen and K. Rypdal, Blow up in nonlinear Schrödinger equations: a general review, Phys. Scr. **33**, 481 (1986).
[11] D. E. Pelinovsky, V. V. Afanasjev, and Yu. S. Kivshar, Nonlinear theory of oscillating, decaying, and collapsing solitons in the generalized nonlinear Schrödinger equation, Phys. Rev. E **53**, 1940 (1996).
[12] D. E. Pelinovsky, Yu. S. Kivshar, and V. V. Afanasjev, Instability-induced dynamics of dark solitons, Phys. Rev. E **54**, 2015 (1996).
[13] D. E. Pelinovsky, A. Buryak, and Yu. S. Kivshar, Instability of solitons governed by quadratic nonlinearities, Phys. Rev. Lett. **75**, 591 (1995).
[14] Y. R. Shen, Self-focusing: experimental, Prog. Quant. Electron. **4**, 1 (1975).

[15] E. L. Dawes and J. H. Marburger, Computer studies in self-focusing, Phys. Rev. **179**, 862 (1969).
[16] D. J. Mitchell and A. W. Snyder, Stability of fundamental nonlinear guided waves, J. Opt. Soc. Am. B **10**, 1572 (1993).
[17] J. E. Bjorkholm and A. Ashkin, cw self-focusing and self-trapping of light in sodium vapour, Phys. Rev. Lett. **32**, 129 (1974).
[18] M. Segev, B. Crosignani, A. Yariv, and B. Fischer, Spatial solitons in photorefractive media, Phys. Rev. Lett. **68**, 932 (1992).
[19] G. Duree, J. L. Shultz, G. Salamo, M. Segev, A. Yariv, B. Crosignani, P. Diporto, E. Sharp, and R. Neurgaonkar, Observation of self-trapping of an optical beam due to the photorefractive effect, Phys. Rev. Lett. **71**, 533 (1993).
[20] G. I. Stegeman and M. Segev, Optical spatial solitons and their interactions: Universality and diversity, Science **286**, 1518 (1999).
[21] S. Trillo and W. Torruellas, Spatial Solitons (Springer, 2001).
[22] A. W. Snyder and D. J. Mitchell, Accessible solitons, Science **276**, 1538 (1997).
[23] P. Yeh, Introduction to Photorefractive Nonlinear Optics (John Wiley & Sons, 1993).
[24] S. Gatz and J. Herrmann, Propagation of optical beams and the properties of two-dimensional spatial solitons in media with a saturable nonlinear refractive index, J. Opt. Soc. Am. B **14**, 1795 (1997).
[25] T. R. Taha and M. J. Ablowitz, Analytical and numerical aspects of certain nonlinear evolution equations, II: Numerical, nonlinear Schrödinger equation, J. Comput. Phys. **55**, 203 (1984).
[26] A. W. Snyder and A. P. Sheppard, Collisions, steering and guidance with spatial solitons, Opt. Lett. **18**, 482 (1993).
[27] V. Tikhonenko, J. Christou, and B. Luther-Davies, Three dimensional bright spatial soliton collison and fusion in a saturable nonlinear medium, Phys. Rev. Lett. **76**, 2698 (1996).
[28] B. Constantini, C. De Angelis, A. Barthelemy, B. Bourliaguet, and V. Kermene, Collisions between type II two-dimensional quadratic solitons, Opt. Lett. **23**, 424 (1998).
[29] M. Shih and M. Segev, Incoherent collisions between two-dimensional bright steady-state photorefractive spatial screening solitons, Opt. Lett. **21**, 1538 (1996).
[30] W. Królikowski, M. Saffman, B. Luther-Davies, and C. Denz, Anomalous interaction of spatial solitons in photorefractive media, Phys. Rev. Lett. **80**, 3240 (1998).
[31] W. Królikowski and S. Holmstrom, Fusion and birth of spatial solitons upon collision, Opt. Lett. **22**, 369 (1997).
[32] W. Królikowski, B. Luther-Davies, C. Denz, and T. Tschudi, Annihilation of photorefractive solitons Opt. Lett. **23**, 97 (1998).
[33] A. W. Snyder, D. J. Mitchell, L. Poladian, and F. Ladouceur, Self-induced optical fibers: spatial solitary waves, Opt. Lett. **16**, 21 (1991).
[34] A. W. Snyder, D. J. Mitchell, and Yu. S. Kivshar, Unification of linear and nonlinear wave optics, Mod. Phys. Lett. B **9**, 1479 (1995).
[35] S. V. Manakov, On the theory of two-dimensional stationary self-focusing of electromagnetic waves, Sov. Phys. JETP **38**, 248 (1974).
[36] J. U. Kang, G. I. Stegeman, J. S. Aitchison, and N. N. Akhmediev, Observation of manakov spatial solitons in AlGaAs planar waveguides, Phys. Rev. Lett. **76**, 3699 (1996).
[37] G. I. Stegeman, W. Torruellas, and Yu. S. Kivshar, in: Spatial Solitons, ch. Quadratic Solitons (Springer, 2001) pp. 127–168.
[38] M. Segev, C. Valley, B. Crosignani, P. Diporto, and A. Yariv, Steady-state spatial screening solitons in photorefractive materials with external applied field, Phys. Rev. Lett. **73**, 3211 (1994).
[39] D. N. Christodoulides and M. I. Carvalho, Bright, dark, and gray spatial soliton states in photorefractive media, J. Opt. Soc. Am. B **12**, 1628 (1995).
[40] M. D. Iturbe Castillo, P. A. Marquez Aguilar, J. J. Sanchez-Mondragon, S. Stepanov, and V. Vysloukh, Spatial solitons in photorefractive $Bi_{12}TiO_{20}$ with drift mechanism of nonlinearity, Appl. Phys. Lett. **64**, 408 (1994).

[41] M. Taya, M. Bashaw, M. M. Fejer, M. Segev, and G. C. Valley, Observation of dark photovoltaic spatial solitons, Phys. Rev. A **52**, 3095 (1995).
[42] M. Taya, M. Bashaw, M. M. Fejer, M. Segev, and G. C. Valley, Y junctions arising from dark-soliton propagation in photovoltaic media, Opt. Lett. **21**, 943 (1996).
[43] A. Ashkin, G. D. Boyd, J. M. Dziedzic, R. G. Smith, A. A. Ballman, J. J. Levinstein, and K. Nassau, Optially induced refractive index inhomogenities in $LiNbO_3$ and $LiTaO_3$, Appl. Phys. Lett. **9**, 72 (1966).
[44] J. Feinberg, Asymmetric self-defocusing of an optical beam from the photorefractive effect, J. Opt. Soc. Am. **72**, 46 (1982).
[45] D. N. Christodoulides and M. I. Carvalho, Compression, self-bending, and collapse of gaussain beams in photorefractive crystals, Opt. Lett. **19**, 1714 (1994).
[46] N. V. Kukhtarev, V. B. Markov, S. G. Odulov, M. S. Soskin, and V. L. Vinetskii, The physics and applications of photorefractive materials, Ferroelectrics **22**, 949 (1979).
[47] A. A. Zozulya and D. Z. Anderson, Propagation of an optical beam in a photorefractive medium in the presence of a photogalvanic nonlinearity or an externally applied electric field, Phys. Rev. A **51**, 1520 (1995).
[48] W. H. Press, S. A. Teukolsky, W. T. Vetterling, and B. P. Flannery, Numerical Recipies in C++ (Cambridge University Press, 2002).
[49] I. V. Petviashvili, On the equation of a nonuniform soliton, Fiz. Plazmy **2**, 469 (1976) [Sov. J. Plasma Phys. **2**, 257 (1976)].
[50] A. A. Zozulya, D. Z. Anderson, A. V. Mamaev, and M. Saffman, Self-focusing and soliton formation in media with anisotropic nonlocal material response, Europhys. Lett. **36**, 419 (1996).
[51] S. Gatz and J. Herrmann, Anisotropy, nonlocality, and space-charge field displacement in (2+1) dimensional self-trapping in biased photorefractive crystals, Opt. Lett. **23**, 1176 (1998).
[52] M. Shih, P. Leach, M. Segev, M. H. Garrett, G. Salamo, and G. C. Valley, Two- dimensional steady state photorefractive solitons, Opt. Lett. **21**, 324 (1996).
[53] M. Shih, M. Segev, G. C. Valley, G. Salamo, B. Crosignani, and P. Di Porto, Observation of two-dimensional steady-state photorefractive screening solitons, Electron. Lett. **31**, 826 (1995).
[54] M. Saffman and A. A. Zozulya, Circular solitons do not exist in photorefractive media, Opt. Lett. **23**, 1579 (1998).
[55] P. A. Marquez Aguilar, J. J. Sanchez Mondragon, S. Stepanov, and V. Vysloukh, Transient self-bending of laser beams in photorefractive crystals with drift nonlinearity, Phys. Rev. A **54** (1996) R2563.
[56] W. Królikowski, N. N. Akhmediev, B. Luther-Davies, and M. Cronin Golomb, Self-bending photorefractive solitons, Phys. Rev. E **54**, 5761 (1996).
[57] J. Petter, C. Weilnau, C. Denz, A. Stepken, and F. Kaiser, Self-bending of photorefractive solitons, Opt. Commun. **170**, 291 (1999).
[58] W. Królikowksi, B. Luther-Davies, C.Denz, J. Petter, C. Weilnau, A. Stepken, and M. R. Belić, Interaction of two-dimensional spatial incoherent solitons in photorefractive media, Appl. Phys. B **68**, 975 (1999).
[59] M. D. Iturbe Castillo, P. A. Marquez Aguilar, J. J. Sanchez-Mondragon, S. Stepanov, and V. Vysloukh, Interferometric measurements of the photoinduced refractive index profiles in photorefractive $Bi_{12}TiO_{20}$ crystals, Opt. Commun. **118**, 515 (1995).
[60] N. J. Zabusky and M. D. Kruskal, Interaction of "solitons" in a collisionless plasma and the recurrence of initial states, Phys. Rev. Lett. **15**, 240 (1965).
[61] J. S. Aitchison, A. M. Weiner, Y. Silberberg, D. E. Leaird, M. K. Oliver, J. L. Jackel, and P. W. Smith, Experimental observation of spatial soliton interactions, Opt. Lett. **16**, 15 (1991).
[62] S. Gatz and J. Herman, Soliton collision and soliton fusion in dispersive materials with a linear and quadratic intensity depending refraction index change, IEEE J. Quantum Electron **28**, 1732 (1992).
[63] F. Reynaud and A. Bartehmeley, Optically controlled interaction between two fundamental soliton beams, Europhys. Lett. **12**, 401 (1990).

[64] V. Tikhonenko, J. Christou, and B. Luther-Davies, Spiraling bright spatial solitons formed by the breakup of an optical vortex in a saturable self-focsusing medium, J. Opt. Soc. Am. B **12**, 2046 (1995).
[65] H. Meng, G. Salamo, M. Shih, and M. Segev, Coherent collisions of photorefractive solitons, Opt. Lett. **22**, 448 (1997).
[66] W. Królikowski, C. Denz, M. Saffman, B. Luther-Davies, and S. Holmstrom, Interaction of coherent and incoherent photorefractive spatial solitons, Asian J. Phys. (1998) 698.
[67] A. Guo, M. Henry, G. Salamo, M. Segev, and G. I. Wood, Fixing multiple waveguides induced by photorefractive solitons: directional couplers and beam splitters, Opt. Lett. **26**, 1274 (2001).
[68] S. Lan, E. DelRe, Z. Chen, M. Shih, and M. Segev, Directional couplers with soliton-induced waveguides, Opt. Lett. **24**, 475 (1999).
[69] M. Shih, M. Segev, and G. Salamo, Circular waveguides induced by two-dimensional bright steady-state photorefractive spatial screening solitons, Opt. Lett. **21**, 931 (1996).
[70] Z. Chen, M. Mitchell, and M. Segev, Steady-state photorefractive soliton-induced Y-junction waveguides and high-order dark spatial solitons, Opt. Lett. **21**, 716 (1996).
[71] J. Petter and C. Denz, Guiding and dividing waves with photorefractive solitons, Opt. Commun. **188**, 55 (2001).
[72] C. Denz, J. Petter, C. Weilnau, and W. Królikowksi, Time-resolved formation and incoherent interaction of photorefractive screening solitons, Phys. Rev. E **60**, 6222 (1999).
[73] L. Poladian, A. W. Snyder, and D. J. Mitchell, Spiralling spatial solitons, Opt. Commun. **85**, 59 (1991).
[74] D. J. Mitchell, A. W. Snyder, and L. Poladian, Interacting self-guided beams viewed as particles: Lorentz force derivation, Phys. Rev. Lett. **77**, 271 (1996).
[75] M. Shih, M. Segev, and G. Salamo, Three-dimensional spiraling of interacting spatial solitons, Phys. Rev. Lett. **78**, 2551 (1997).
[76] A. V. Buryak, Yu. S. Kivshar, M. Shih, and M. Segev, Induced coherence and stable soliton spiraling, Phys. Rev. Lett. **82**, 81 (1999).
[77] A. Stepken, M. R. Belić, F. Kaiser, W. Królikowski, and B. Luther-Davies, Three dimensional trajectories of interacting incoherent photorefractive solitons, Phys. Rev. Lett. **82**, 540 (1998).
[78] M. R. Belić, A. Stepken, and F. Kaiser, Spiraling behaviour of photorefractive screening solitons, Phys. Rev. Lett. **82**, 544 (1999).
[79] N. S. Kapany and J. J. Burke, Optical Waveguides (Academic, New York, 1972).
[80] R. De La Fuente, A. Barthelemy, and C. Froehly, Spatial soliton-induced guided waves in a homogeneous nonlinear kerr medium, Opt. Lett. **16**, 793 (1991).
[81] B. Luther-Davies and X. Yang, Waveguides and Y junctions formed in bulk media by using dark spatial ssolitons, Opt. Lett. **17**, 1755 (1992).
[82] M. Morin, G. Duree, G. Salamo, and M. Segev, Waveguides formed by quasi-steady-state photorefractive spatial solitons, Opt. Lett. **20**, 2066 (1995).
[83] J. Petter, C. Denz, A. Stepken, and F. Kaiser, Anisotropic waveguides induced by photorefractive (2+1)d solitons, J. Opt. Soc. Am. B **19**, 1145 (2002).
[84] M. Klotz, H. Meng, G. J. Salamo, M. Segev, and S. R. Montgomery, Fixing the photorefractive soliton, Opt. Lett. **24**, 77 (1999).
[85] M. Shih, Z. Chen, M. Mitchell, M. Segev, H. Lee, R. S. Feigelson, and J. P. Wilde, Waveguides induced by photorefractive screening solitons, J. Opt. Soc. Am. B **14**, 3091 (1997).
[86] A. Bramati, W. Chinaglia, S. Minardi, and P. Di Trapani, Reconstruction of blurred images by controlled formation of spatial solitons, Opt. Lett. **26**, 1409 (2002).
[87] M. Soljačić, S. Sears and M. Segev, Self-trapping of "necklace" beams in self-focusing kerr media, Phys. Rev. Lett. **81**, 4851 (1998).
[88] D. N. Christodoulides, S. R. Singh, and M. I. Carvalho, Incoherently coupled soliton pairs in biased photorefractive crystals, Appl. Phys. Lett. **68**, 1763 (1996).
[89] Z. Chen, M. Segev, T. H. Coskun, and D. N. Christodoulides, Observation of incoherently coupled photorefractive spatial soliton pairs, Opt. Lett. **21**, 1436 (1996).

[90] M. Mitchell, M. Segev, and D. N. Christodoulides, Observation of multihump multimode solitons, Phys. Rev. Lett. **80**, 4657 (1998).
[91] E. A. Ostrovskaya, Yu. S. Kivshar,D. V. Skryabin, and W. J. Firth, Stability of multihump optical solitons, Phys. Rev. Lett. **83** (1999).
[92] E. A. Ostrovskaya and Yu. S. Kivshar, Multi-hump optical solitons in a saturable medium, J. Opt. B **1** (1999).
[93] Z. H. Musslimani, M. Segev, D. N. Christodoulides, and M. Soljačić, Composite multihump vector solitons carrying topological charge, Phys. Rev. Lett. **84**, 1164 (2000).
[94] Z. H. Musslimani, M. Segev, and D. N. Christodoulides, Multicomponent two-dimensional solitons carrying topological charges, Opt. Lett. **25**, 61 (2000).
[95] J. J. García-Ripoll, V. M. Pérez-García, E. A. Ostrovskaya, and Yu. S. Kivshar, Dipole-mode vector solitons, Phys. Rev. Lett. **85**, 82 (2000).
[96] W. Królikowski, E. A. Ostrovskaya, C. Weilnau, M. Geisser, G. McCarthy, Yu. S. Kivshar, C. Denz, and B. Luther-Davies, Observation of dipole-mode vector solitons, Phys. Rev. Lett. **85** (2000).
[97] T. Carmon, C. Anastassiou, S. Lan, D. Kip, Z. H. Musslimani, and M. Segev, Observation of two-dimensional mulitmode solitons, Opt. Lett. **25**, 1113 (2000).
[98] K. Motzek, A. Stepken, F. Kaiser, M. R. Belić, M. Ahles, C. Weilnau, and C. Denz, Dipole-mode vector solitons in anisotropic photorefractive media, Opt. Commun. **197** (2001).
[99] C. Weilnau, W. Królikowski, E. A. Ostrovskaya, M. Ahles, M. Geisser, G. McCarthy, C. Denz, Yu. S. Kivshar, and B. Luther-Davies, Composite spatial solitons in saturable nonlinear bulk medium, Appl. Phys. B **72** (2001).
[100] D. Neshev, G. McCarthy, W. Królikowski, E. A. Ostrovskaya, Yu. S. Kivshar, G. F. Calvo, and F. Agullo-Lopez, Dipole-mode vector solitons in anisotropic nonlocal self-focusing media, Opt. Lett. **26**, 1185 (2001).
[101] I. V. Basistiy, M. S. Soskin, and M. V. Vasnetsov, Optical wavefront dislocation and their properties, Opt. Commun. **119**, 604 (1995).
[102] A. V. Mamaev, M. Saffman, and A. A. Zozulya, Decay of high order optical vortices in anisotropic nonlinear optical media, Phys. Rev. Lett. **78**, 2108 (1997).
[103] M. R. Belić, D. Vujić, A. Stepken, F. Kaiser, G.F. Calvo, F. Agulló-López, and M. Carrascosa, Isotropic versus anisotropic modeling of photorefractive solitons, Phys. Rev. E **65**, 066610 (2002).
[104] A. V. Mamaev, A. A. Zozulya, V. K. Mezentsev, D. Z. Anderson, and M. Saffman, Bound dipole solitary solutions in anisotropic nonlocal self-focusing media, Phys. Rev. A **56** (1997) R1110.
[105] C. Weilnau, C. Denz, M. Ahles, A. Stepken, K. Motzek, and F. Kaiser, Generation of higher-order optical (2+1) dimensional spatial vector solitons in a nonlinear anisotropic medium, Phys. Rev. E **64** (2001).
[106] A. S. Desyatnikov, D. Neshev, E. A. Ostrovskaya, Yu. S. Kivshar, G. McCarthy, W. Królikowski, and B. Luther-Davies, Multipole composite spatial solitons:theory and experiment, J. Opt. Soc. Am. B **19**, 586 (2002).
[107] A. S. Desyatnikov, D. Neshev, E. A. Ostrovskaya, Yu. S. Kivshar, W. Królikowski, B. Luther-Davies, J. J. García-Ripoll, and V. M. Pérez-García, Multipole spatial vector solitons, Opt. Lett. **26**, 435 (2001).
[108] K. Motzek, unpublished, TU-Darmstadt, 2001.
[109] A. S. Desyatnikov and Yu. S. Kivshar, Necklace-ring vector solitons, Phys. Rev. Lett. **87**, 033901 (2001).
[110] M. Ahles, K. Motzek, A. Stepken, F. Kaiser, C. Weilnau, and C. Denz, Stabilization and breakup of coupled dipole-mode beams in an anisotropic nonlinear medium, J. Opt. Soc. Am. B **19**, 557 (2002).
[111] A. S. Desyatnikov, Yu. S. Kivshar, K. Motzek, F. Kaiser, C. Weilnau, and C. Denz, Multicomponent dipole-mode spatial solitons, Opt. Lett. **27**, 634 (2002).

[112] T. Carmon, C. Pigier, Z. H. Musslimani, M. Segev, and A. Nepomnyashchy, Rotating propeller solitons, Phys. Rev. Lett. **87**, 143901 (2001).
[113] K. Motzek, F. Kaiser, C. Weilnau, C. Denz, G. McCarthy, W. Królikowski, A. S. Desyatnikov, and Yu. S. Kivshar, Multi-component vector solitons on photorefractive crystals, Opt. Commun. (2002) [to be published, August 2002].
[114] A. S. Desyatnikov and Yu. S. Kivshar, Rotating optical soliton clusters, Phys. Rev. Lett. **88**, 053901 (2002).
[115] M. Mitchell, M. Segev, T. H. Coskun, and D. N. Christodoulides, Theory of self-trapped spatially incoherent light beams, Phys. Rev. Lett. **79**, 4990 (1997).
[116] M. Mitchell Z. Chen, M. Shih, and M. Segev, Self-trapping of partially spatially incoherent light, Phys. Rev. Lett. **77**, 490 (1996).
[117] D. Kip, C. Anastassiou, E. Eugenieva, D. N. Christodoulides, and M. Segev, Transmission of images through highly nonlinear media by gradient-index lenses formed by incoherent solitons, Opt. Lett. **26**, 524 (2001).
[118] D. Kip, M. Soljačić, M. Segev, E. Eugenieva, and D. N. Christodoulides, Modulation instability and pattern formation in spatially incoherent light beams, Science **290**, 495 (2000).
[119] M. Mitchell and M. Segev, Self-trapping of incoherent white light, Nature **387**, 880 (1997).